Effects of heating and copper diffusion on feldspar

An on-going research

Kamolwan Thirangoon
GIA Laboratory, Bangkok

Updated April 29, 2009

Abstract

Heat treatment was conducted on light yellow feldspar from Plush and Ponderosa, Oregon, USA, Mexico and China. The study was performed to monitor chemical and physical changes of the materials involved. It was shown that simple heat treatment at 1200 °C for 50 hours in air caused some changes in chemical composition and inclusion suite. In addition, heating also creates internal diffusion of the metallic copper that gives rise to schiller effect.

Introduction

Red andesine was an official gemstone for the Chinese Olympic Games in 2008. For many years this red feldspar was known as a rare material. Obtained mainly from Oregon USA, only small quantities of this material were available in the market. In 2002, gem-quality red feldspar said to be from Congo appeared in the market. These were up to 30 carats in size and internally very clean. The Congo material was reported to come from an area about 100 kilometers South West of Goma. However, the existence of the mine could not be validated. In 2005, a large number of red feldspars were marketed as “Chinese Andesine” in the Tucson Gem Shows. In 2006, the stones appeared again at the Tucson shows, this time they were marketed as

"Tibet sunstone". This led to concerns being expressed in the trade and speculation that the stones had been treated (to improve or change the color) in some manner.

The feldspar-group of minerals are silicates and are abundant in earth's crust (Mernagh. 1991, Freeman, Wang, Kuebler, Jolliff and Haskin. 2008). This group is characterized in accordance with their chemical composition and structural state (Mernagh. 1991). Based on the proportion of K, Na and Ca, feldspar can be classified further into two main groups; alkaline feldspar and plagioclase feldspar. Alkaline feldspars are those in the series between $KAlSi_3O_8$ and $NaAlSi_3O_8$. While plagioclase feldspar are in the series between $NaAlSi_3O_8$ and $CaAl_2\ Si_2O_8$ (Mernagh. 1991). Plagioclase feldspar can be further divided into 6 subgroups as follows; albite, oligoclase, andesine, labradorite, bytownite and anorthite (Figure 1).

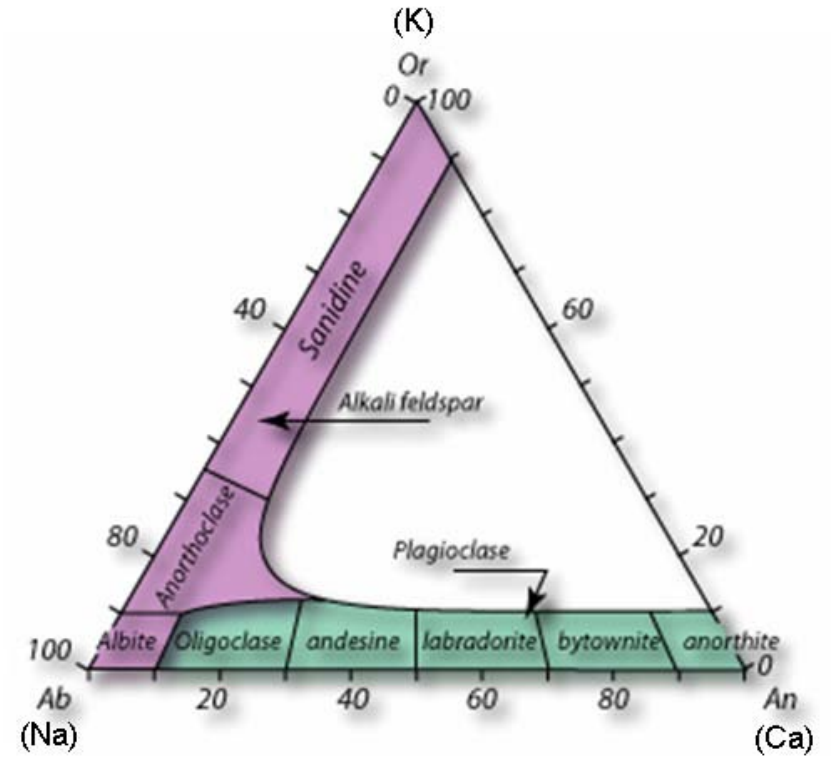

Figure 1 Standard ternary feldspar diagram shows the chemical composition of feldspar varieties.

The red color causing agent or chromophore in labradorite is Cu. Depending on the Cu^0 particle size, concentration of Cu and the temperature at which exsolution is initiated, a red coloration or schiller effect can be achieved (Hofmeister and Rossman. 1985). Red coloration is caused by intrinsic absorption of colloidal Cu^0 particles that are too small to scatter light whereas schiller occurs when Cu^0 particles exist in a larger size. (Hofmeister and Rossman. 1985).

The overall goal of this study is to monitor changes in feldspar following heat treatment and the diffusion of Cu. The selected materials are from two well-known sources in Oregon, Plush and Ponderosa, as well as materials from Mexico and China. The optical and chemical properties of the unheated start material were recorded in detail. Their inclusion suite and basic gemological properties were also observed and recorded. The materials were then subjected to a heating scenario (this is presently

being followed by diffusion with Cu, the results of which will be release later). After treatment all the data was re-taken and compared with the original data from the untreated stage (this will also be done following Cu diffusion).

This part of the study detailed here focuses on the effects of heat treatment (alone) on the start material. The chemistry of the unheated material was also compared with material from Tibet provided by Ahmadjan Abduriyim from Gemmological Association of all Japan.

Materials and Methods

Thirty-nine light yellow feldspar samples were acquired from John Emmett of Crystal Chemistry, Brush Prairie, Washington, for this study. They are from four different sources; Plush, Oregon, USA (8 pieces), Ponderosa, Oregon, USA (9 pieces), China (7 pieces) and Mexico (15 pieces). Examples of material used in this study are shown in Figure 2, Figure 3, Figure 4, Figure 5 and Figure 6. Prior to acquisition they were fabricated into polished plates by John Emmett. The unheated samples range in size from 3.22 to 11.59 cts and are 2.73 to 4.18 mm thick. The heating experiment conducted by John Emmett involved heating each sample at 1200 °C in air for 50 hours on an alumina felt in a furnace. The temperature of 1200 °C is below the solidus line at 50% anorthite and the 50 hours duration time is less than the time required for Cu diffusion. After heating and repolishing the samples ranged in size from 3.18 to 11.06 cts and were 2.69 to 3.97 mm thick. Two red and one yellow labradorite rough acquired from Ahmadjan Abduriyim were included in this study. All samples were washed with acetone and aqua regia in an ultrasonic bath for the total time of 3 minutes in each solution prior to testing.

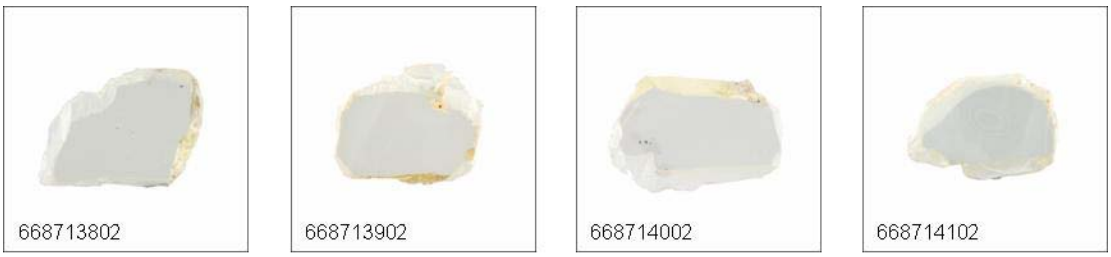

Figure 2: Examples of unheated samples from Mexico. Photo by Suchada Kittayachaiwattana and Adirote Sripradi

Figure 3: Examples of unheated samples from Plush, Oregon, USA. Photo by Suchada Kittayachaiwattana and Adirote Sripradi

Figure 4: Examples of unheated samples from Ponderosa, Oregon, USA. Photo by Suchada Kittayachaiwattana and Adirote Sripradi

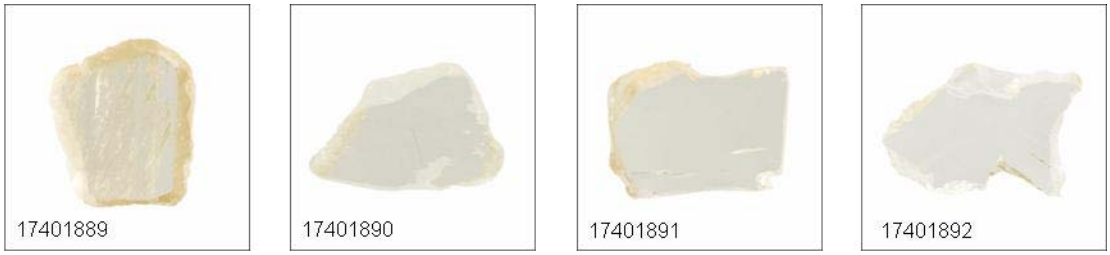

Figure 5: Examples of unheated samples from China. Photo by Suchada Kittayachaiwattana and Adirote Sripradi

Figure 6: Samples from Tibet. Photo by Suchada Kittayachaiwattana and Adirote Sripradi

Refractive indices were measured with a standard gem refractometer using a monochromatic light that simulates the light produced by a sodium arc lamp; Specific Gravity (S.G.), determinations were calculated by the hydrostatic technique using an appropriately fitted Mettler electronic balance with water at room temperature; UV, fluorescence was observed using a UVP, UVLS-28 EL series, 8 watt, UV lamp with both 365 and 254nm radiation; Microscopic observations were made using various GIA Gemolite microscopes at between 10 and 65x magnifications; Raman spectra were collected using a Renishaw inVia Raman microscope fitted with a 514 nm Argon Ion laser; Infrared spectra were collected using a Thermo Nicolet 6700 FTIR and appropriate accessories; UV/visible/NIR spectra were collected using a Perkin Elmer Lambda 950 spectrophotometer with various bench configurations and dual polarizers; Chemical analysis was performed using an Thermo X-Series II Laser Ablation Inductive Plasma Mass Spectroscopy (LA-ICP-MS) system attached to a New Wave research UP-213 laser system.

Results

While changes were observed after heating, the sample appearance showed no apparent improvement. The samples became a little more yellowish and less transparent (Figure 7, Figure 8, and Figure 9). Some of the samples from Plush, Oregon, exhibited red schiller cloud before the heating experiment. After heating the red color disappeared and the cloud appeared white along with other changes in their inclusion suites. Examples of inclusions observed after heating include discoid fractures coming off small string of crystals, reflective leaf-like inclusions, a disintegrated black crystal, a deformed crystal with tension fractures, and the fusion of reflective ovoid plates of possible peristerite (See Inclusion suite, page24).

It seems that chemical composition of the samples was also altered by heating. Samples from Plush, Oregon were identified as labradorite before heating but as bytownite after heating. Some of the samples from China were identified as andesine before heating but labradorite after heating, See Table 1. In addition, the Cu concentration in the red cloud areas diffused to other area of the samples resulting in a more even distribution of the Cu content throughout.

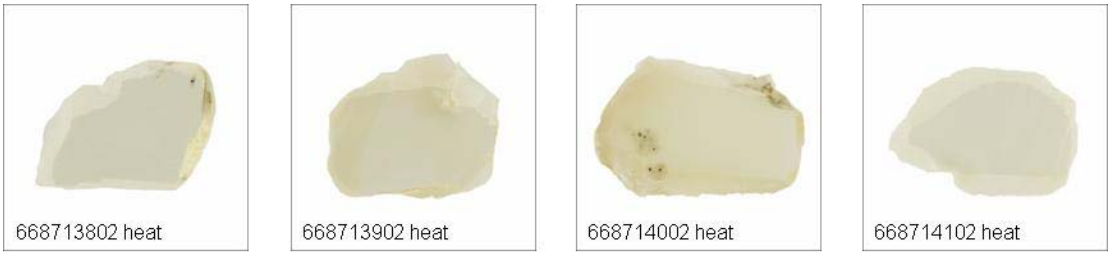

Figure 7 Examples of heated samples from Mexico. Photo by Suchada Kittayachaiwattana and Adirote Sripradi

Figure 8 Examples of heated samples from Plush, Oregon. Photo by Suchada Kittayachaiwattana and Adirote Sripradi

Figure 9 Examples of heated samples from China. Photo by Suchada Kittayachaiwattana and Adirote Sripradi

Table 1: Feldspar variety determination and cloud appearance of the samples before and after heating experiment. Red cloud refers to red schiller cloud of ^{0}Cu. White cloud refers to dense cloud of minute particles. Samples from Ponderosa and Tibet have not been subjected to heat treatment at this time. The analysis was performed on sample 17401909 red (-R) and colorless (-C) zone. Sample 17401910 is light yellow (-Y) in color.

Source	Samples	Feldspar variety		Cloud appearance			
		before heating	after heating	Before heating		after heating	
				White	Red	White	Red
Mexico	668713802	labradorite	labradorite	x		x	
	668713902	labradorite	labradorite	x		x	
	668714002	labradorite	labradorite	x		x	
	668714102	labradorite	labradorite	x		x	
	668714202	labradorite	labradorite	x		x	
	668714302	labradorite	labradorite	x			
	668714402	labradorite	labradorite	x		x	
	668714502	labradorite	labradorite	x		x	
	668714602	labradorite	labradorite	x		x	
	668714702	labradorite	bytownite	x		x	
	668714802	labradorite	labradorite				
	668714902	labradorite	labradorite	x		x	
	668715002	labradorite	labradorite	x		x	
	668715102	labradorite	labradorite	x		x	
	668715202	labradorite	labradorite	x		x	
Ponderosa	668119202	bytownite		x			
	668119302	bytownite		x			
	668119402	bytownite		x			
	668119502	bytownite		x			
	668119602	bytownite		x			
	668119702	bytownite		x			
	668119802	bytownite		x	x		
	668119902	bytownite		x			
	668120002	bytownite		x	x		
Plush	668715302	labradorite	bytownite	x	x	x	
	668715402	labradorite	bytownite	x		x	
	668715502	labradorite	bytownite	x		x	
	668715602	labradorite	bytownite	x		x	
	668715702	labradorite	bytownite	x		x	
	668715802	labradorite	bytownite	x		x	
	668715902	labradorite	bytownite	x	x	x	
	668716002	labradorite	bytownite	x	x	x	
China	17401889	labradorite	labradorite				
	17401890	labradorite	labradorite				
	17401891	labradorite	labradorite	x		x	
	17401892	andesine	labradorite				
	17401893	labradorite	labradorite				
	17401894	andesine	labradorite	x		x	
	17401895	labradorite	labradorite	x		x	
Tibet	17401909-R	labradorite					
	17401909-C	labradorite					
	17401910-Y	labradorite					

Chemical analysis

Chemical analysis was performed using Laser Ablation-Inductively coupled Plasma Mass Spectroscopy (LA-ICP-MS). Samples were cleaned with acetone and aqua regia in an ultrasonic bath to eliminate surface contamination prior to the analysis. The laser operated at a wavelength of 213 nm with He as the carrier gas. Laser-ablation parameters were as follows: 40 µm spot diameter, ~10 J/cm2 laser energy density (fluence), 7 Hz repetition rate and 40 second laser dwell time. Each sample was ablated between 19 to 52 spots. NIST SRM 610, 612 (Pearce. 1996) were used as external standards.

Cu mapping: internal diffusion of intrinsic Cu due to heat treatment

Mapping analysis using LA-ICP-MS method was performed in all samples to examine the distribution of Cu through the sample. Two unheated samples from Plush, Oregon showed red schiller cloud of Cu platelets. Chemistry analysis revealed that Cu is more concentrated in the red cloud area. Sample 68715902 showed average 63Cu, 65Cu concentration of 17.74, 17.61 ppmw and 18.71, 18.12 ppmw before and after the heat treatment, respectively. Figure 10 shows that prior to heating Cu is concentrated only in the red cloud area. Outside the cloud, Cu was not detected. However, after heating, the red coloration disappeared but the cloud remained. The Cu concentration in the cloud area decreased while Cu concentration in the area that previously did not contain Cu increased (Figure 11).

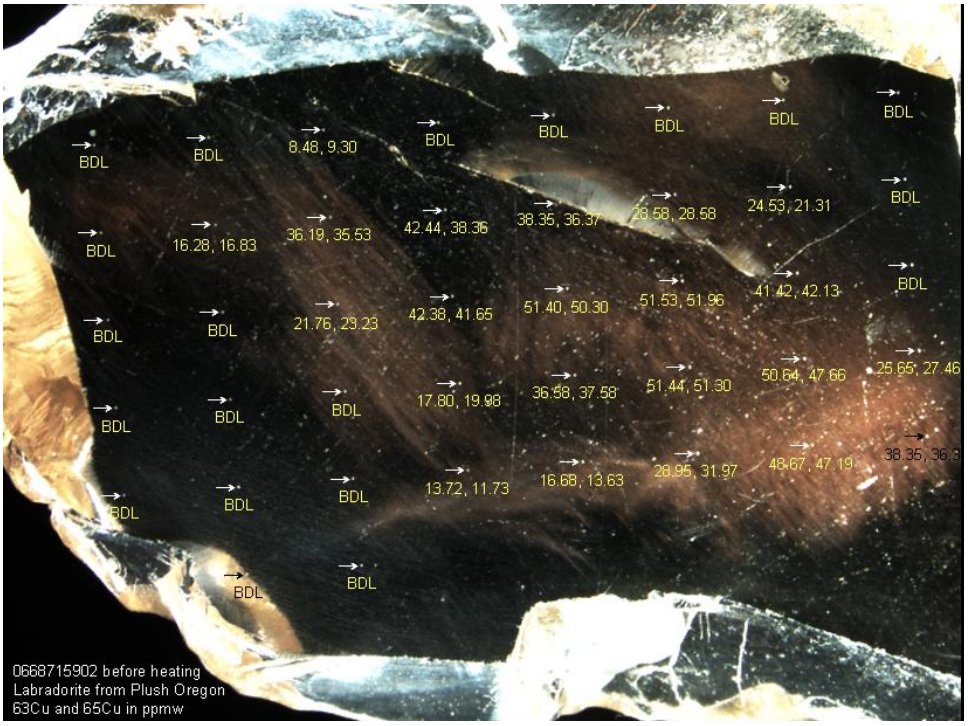

Figure 10: Cu mapping of (668715902) labradorite from Plush, Oregon, USA before heating experiment. The ^{63}Cu and ^{65}Cu concentration are shown in ppmw. Cu concentration in the zone with red schiller is much higher than the zone without the red schiller cloud which Cu was not detected. (BDL= Below Detection Limit).

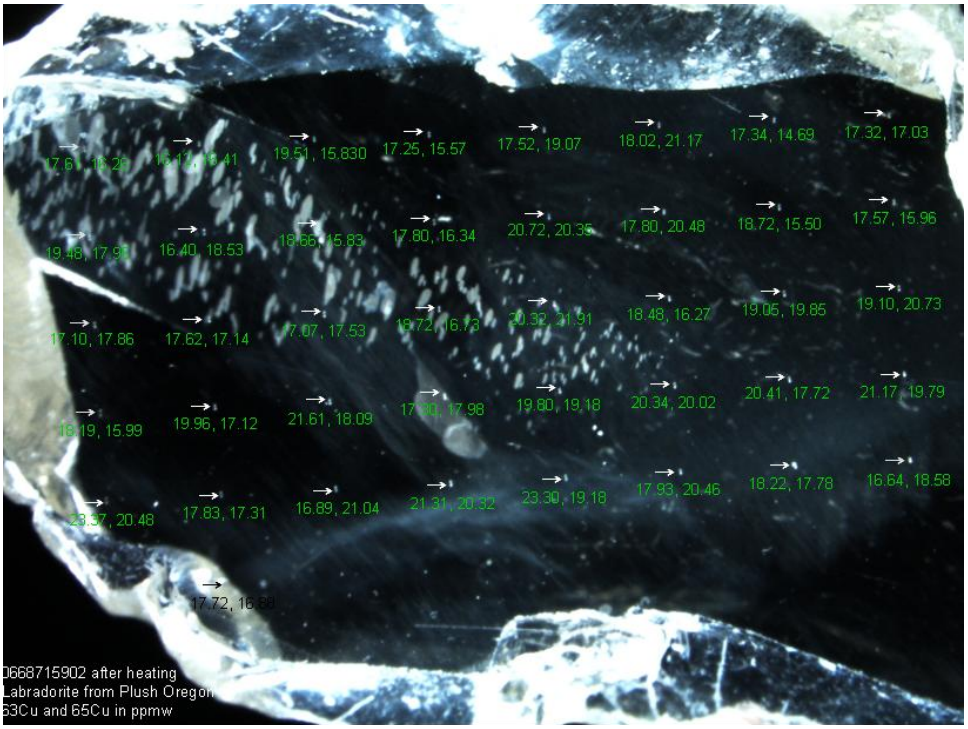

Figure 11: Cu mapping of (668715902) labradorite from Plush, Oregon, USA after heating experiment. The ^{63}Cu and ^{65}Cu concentration are shown in ppmw. Cu concentration is evenly distributed through out the sample. Note that the red schiller cloud has changed into white cloud. There are discoid fractures on the left of the sample where it was strings of transparent crystals.

The same phenomenon was observed in sample 68715302 from Plush, Oregon. The average 63Cu, 65Cu concentration is 19.44, 19.26 ppmw and 15.07, 15.14 ppmw before and after the heat treatment, respectively. Before heating, Cu concentration is higher in the red cloud area and lower in the area further away from the cloud (Figure 12). After heating, the concentration in the cloud area which has lost the red coloration decreased and Cu content is more evenly distributed in all area (Figure 13).

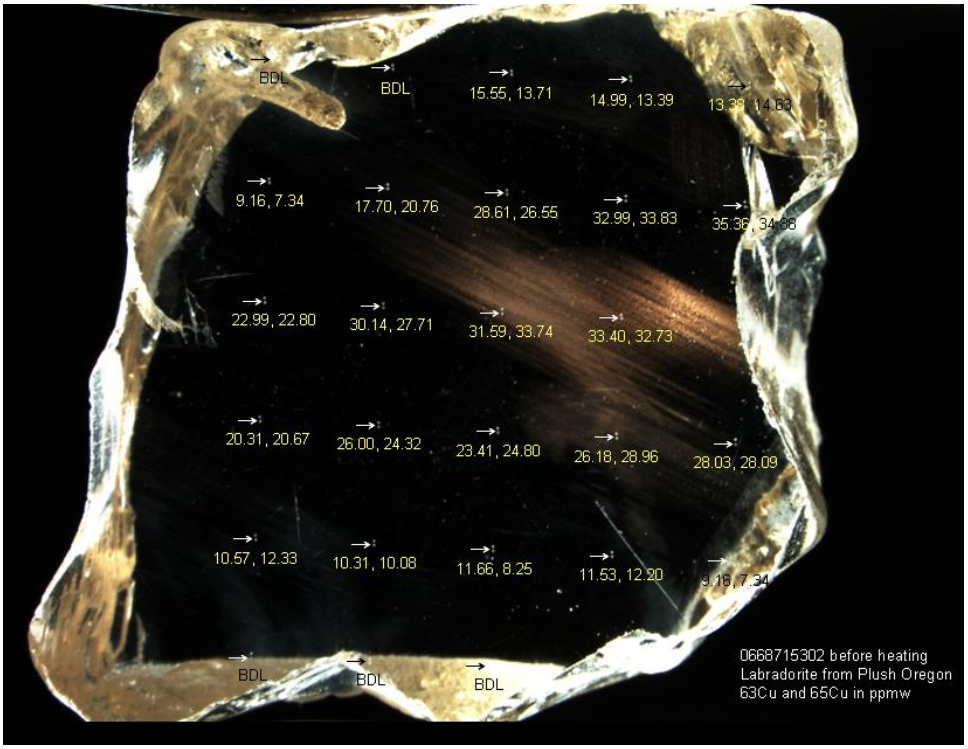

Figure 12: Cu mapping of (668715302) labradorite from Plush, Oregon, USA before heating experiment. The ^{63}Cu and ^{65}Cu concentration are shown in ppmw. Cu concentration in the zone with red schiller is much higher than the zone without schiller cloud. (BDL= Below Detection Limit).

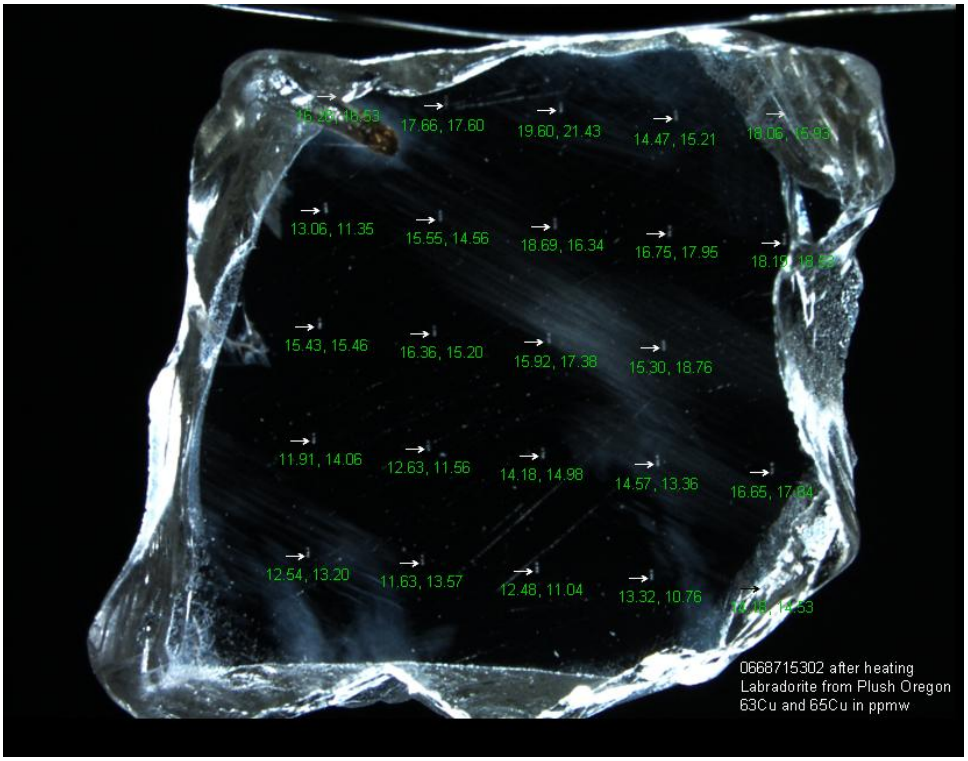

Figure 13: Cu mapping of (668715302) labradorite from Plush, Oregon, USA after heating experiment. The ^{63}Cu and ^{65}Cu concentration are shown in ppmw. Cu concentration is evenly distributed through out the sample. Note that the red schiller cloud has lost its red coloration.

The results indicate that there is an internal diffusion of intrinsic Cu due to heating at 1200 °C for 50 hours. However, the internal diffusion did not improve coloration and the appearance of the samples. The average Cu concentration of the samples remains the same after heating confirming that there is no external diffusion of Cu.

Population field

Major and trace elements found are shown in Table 2. The major elements are Na, K and Ca. The trace elements present are Mg, Ti, Mn, Fe, Cu, Ga, Sr, Ba, La and Ce. The element La and Ce exist at lower than 1.5 and 2 ppmw, respectively. Feldspar from Tibet also contains a few other elements including Li (16-33 ppmw), S (2900-12600 ppmw), V (160-1600 ppmw) and less than a ppmw of Pr, Nd and Eu.

Only samples from Ponderosa, Plush and Tibet contain Cu. The samples from China and Mexico do not have detectable levels of Cu. Samples from China and Tibet are similar in their chemistry except that the samples from Tibet contain Cu. The sample 17401909 which is red in color has high concentration of Cu (470-640 ppmw). The sample 17401910 which is light yellow in color has about 10 and 17 ppmw of ^{63}Cu and ^{65}Cu. Samples from Ponderosa and Plush contain from 3 to 33 ppmw of Cu (Table 2). Samples with red schiller cloud from Plush are 668715302, 668715902 and 6687156002, from Ponderosa are 668119802 and 668120002 (Table 1). However, they do not necessarily contain the highest average level of Cu since this depends on the size of the cloud area and the numbers of spots analyzed that are in the red cloud area versus the area without the cloud.

Table 2 shows that samples from different sources have different level of the main and trace elements. Samples from Ponderosa and Plush, Oregon seems to have higher Mg content than samples from other sources. Samples from China and Tibet have the highest level of Na, 26000-31000 ppmw, followed by Mexico, (23000-26000 ppmw), Plush, (21000-24000 ppmw) and Ponderosa with the least amount of Na, (~15000 ppmw). Samples from China and Tibet have the highest levels of K (~2000-3000 ppmw), followed by Mexico (1600-2000 ppmw) then Plush (700-800 ppmw) and Ponderosa (~300 ppmw). Samples from Ponderosa tend to have a lower level of several trace elements which are K, Na, Ti, Ga, Sr and Ba (Table 1). Samples from China tend to have lower Ca content comparing to samples from other sources including samples from Tibet. This implies that Ca could be a key element in separating samples from Tibet from China. However, further investigation is required. Chemical analysis must be done on more samples from Tibet. The difference in their elemental concentration can be used in population field plot as shown in Figure 14 to 17.

Table 2: Average concentration of major and trace elements of the unheated samples from LA-ICP-MS analysis in ppmw. The number of spots ranging from 6 to 54 spots per sample. Samples from Mexico, Ponderosa, Plush and China are light yellow in color. Only two samples from Tibet were analyzed. The analysis was performed on sample 17401909 red (-R) and colorless (-C) zone. Sample 17401910 is light yellow (-Y) in color.

Sources	Samples	23Na	24Mg	39K	44Ca	47Ti	55Mn	56Fe	63Cu	65Cu	69Ga	88Sr	137Ba
Mexico	668713802	26123.10	491.08	1845.72	67069.66	273.32	29.67	1983.07	0.00	0.00	16.58	691.70	86.72
	668713902	23305.00	477.68	1586.00	64486.11	264.17	29.44	1887.50	0.00	0.00	15.73	684.88	80.75
	668714002	25553.68	500.17	1761.74	66291.58	294.41	29.50	2031.53	0.00	0.00	18.35	730.79	101.69
	668714102	28192.63	561.71	2015.05	75772.63	305.20	34.62	2203.58	0.00	0.00	17.52	797.74	91.00
	668714202	26252.86	512.05	1930.52	67160.95	279.72	30.54	1966.43	0.00	0.00	16.23	708.41	85.37
	668714302	27048.64	496.36	1867.18	69113.18	271.28	30.04	1997.64	0.00	0.00	18.34	725.79	89.24
	668714402	25626.80	485.04	1751.04	67355.20	268.72	30.01	1933.84	0.00	0.00	16.13	720.20	85.94
	668714502	24828.18	495.53	1657.00	66269.09	279.07	30.33	1976.95	0.00	0.00	15.22	732.37	90.75
	668714602	24309.38	495.24	1667.13	62740.63	273.35	29.70	1978.69	0.00	0.00	15.05	704.28	93.51
	668714702	26643.64	524.32	1917.64	68069.09	302.24	32.71	2093.23	0.00	0.00	19.57	751.73	95.22
	668714802	26825.50	520.91	1940.60	66664.50	286.67	30.86	1987.10	0.00	0.00	18.87	717.94	86.62
	668714902	24942.73	478.79	1827.86	63931.82	280.22	28.83	1890.05	0.00	0.00	15.90	706.34	89.12
	668715002	24187.83	480.47	1699.04	64403.91	270.59	28.88	1817.57	0.00	0.00	15.25	692.21	83.72
	668715102	25406.25	467.00	1776.54	63746.25	266.16	29.98	1925.13	0.00	0.00	15.84	701.88	89.58
	668715202	22725.83	476.25	1586.04	61864.58	262.97	29.64	1934.33	0.00	0.00	14.24	707.89	81.98
Ponderosa	668119202	15431.00	776.23	288.36	73883.00	124.34	33.20	1948.10	18.52	18.92	9.18	332.57	8.82
	668119302	15006.50	752.95	295.97	75160.50	122.74	34.11	2006.10	4.17	5.01	9.28	329.80	8.10
	668119402	14470.71	761.00	332.59	71025.00	131.11	34.54	2075.29	33.61	33.42	9.74	342.37	11.60
	668119502	13574.58	753.57	296.96	73875.83	129.23	34.91	2086.63	2.97	2.84	10.04	296.08	10.04
	668119602	15081.90	809.28	287.42	79678.57	134.31	35.01	2039.81	16.58	16.75	9.73	348.32	8.76
	668119702	15811.43	763.56	333.16	78397.62	134.73	35.34	2098.71	8.79	8.97	10.10	348.58	10.28
	668119802	14010.00	792.77	293.51	75295.33	124.55	34.22	1980.60	19.69	19.66	9.00	327.19	8.40
	668119902	14800.48	736.06	341.56	73073.81	136.89	33.51	2051.62	3.68	3.83	9.78	338.66	10.79
	668120002	15168.95	738.78	302.90	76964.74	122.45	31.88	1943.47	5.08	5.04	8.95	305.58	7.69
Plush	668715302	22240.37	657.43	736.11	75888.52	164.67	36.29	2412.04	21.21	21.01	14.32	457.37	46.12
	668715402	21204.17	629.83	795.73	73500.00	165.29	34.90	2304.97	13.01	13.21	13.92	445.79	45.54
	668715502	21477.69	618.89	746.40	75747.18	167.25	34.70	2254.46	12.64	12.32	13.67	468.78	45.40
	668715602	21729.76	653.39	741.64	77311.95	174.04	36.19	2531.34	14.46	14.41	14.11	426.39	44.63
	668715702	22766.75	634.06	739.39	73881.00	156.03	33.80	2346.48	13.42	13.41	13.34	399.50	42.47
	668715802	23534.00	638.90	778.33	77977.50	161.05	35.31	2285.40	8.91	9.40	13.40	462.64	45.54
	668715902	21276.43	633.31	766.58	70182.62	162.67	34.26	2277.00	33.06	32.81	13.23	427.05	45.82
	668716002	24100.36	674.15	858.62	77349.64	183.18	37.83	2638.14	23.62	24.32	14.68	512.69	55.25
China	17401889	31072.69	341.37	2770.23	52480.00	275.74	24.53	1837.96	0.00	0.00	18.42	814.09	91.18
	17401890	28737.14	322.01	2472.86	49222.50	254.79	22.94	1654.46	0.00	0.00	16.29	748.64	77.00
	17401891	27410.59	283.30	2759.21	45877.35	225.04	22.00	1857.76	0.00	0.00	16.23	718.63	84.73
	17401892	26338.44	291.69	2606.24	42706.67	223.24	20.94	1691.78	0.00	0.00	16.78	700.24	84.88
	17401893	26743.33	322.71	2603.22	47096.11	228.66	23.03	1630.00	0.00	0.00	15.61	735.70	68.72
	17401894	27100.56	280.56	2568.85	43166.30	212.54	20.16	1638.52	0.00	0.00	15.31	678.73	78.94
	17401895	30670.91	342.27	2723.36	50814.55	258.25	23.39	1905.18	0.00	0.00	17.86	792.26	93.92
Tibet	17401909-R	26034.13	310.53	3261.15	60848.04	269.31	28.63	1727.17	471.66	467.08	16.84	809.09	76.68
	17401909-C	27635.45	346.10	2550.55	55569.09	262.55	24.20	1725.64	639.20	637.08	16.94	788.34	77.63
	17401910-Y	27016.80	324.79	55764.80	257.08	23.53	314.97	319.18	10.17	17.03	10.69	72.58	0.86

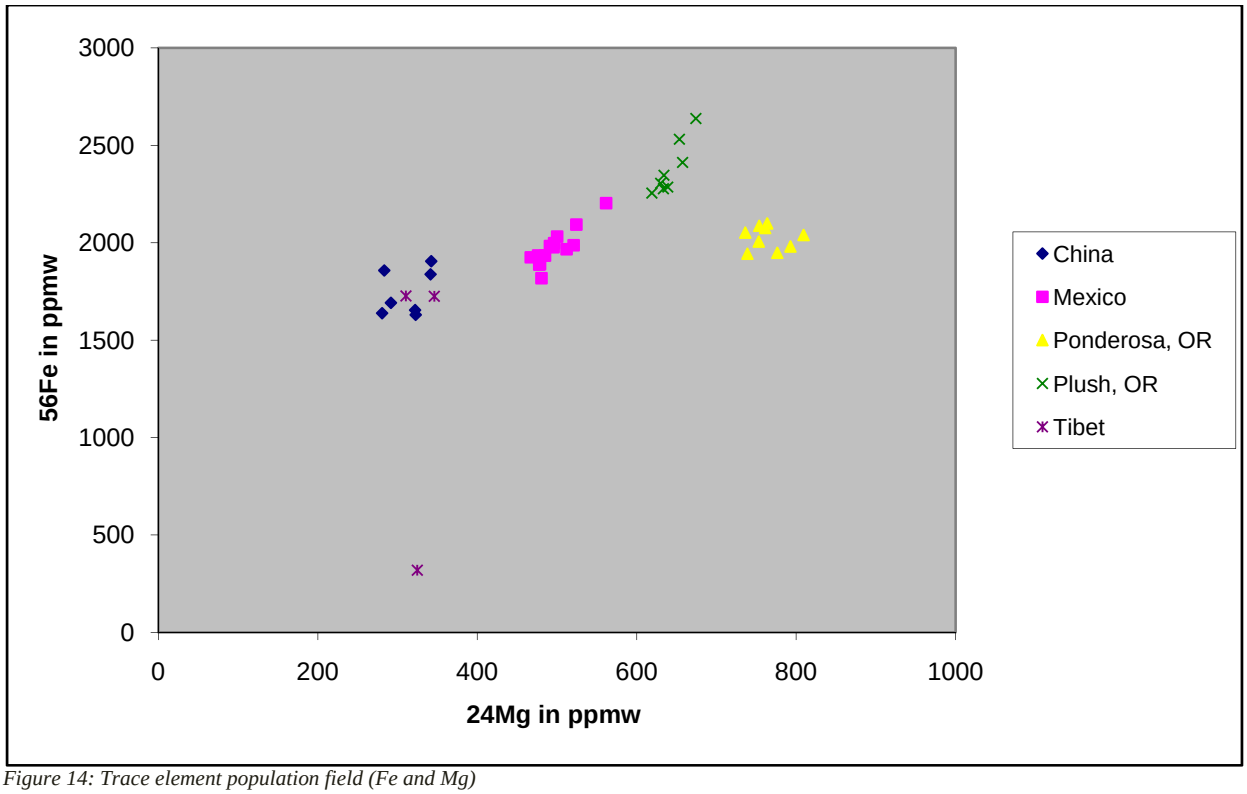

Figure 14: Trace element population field (Fe and Mg)

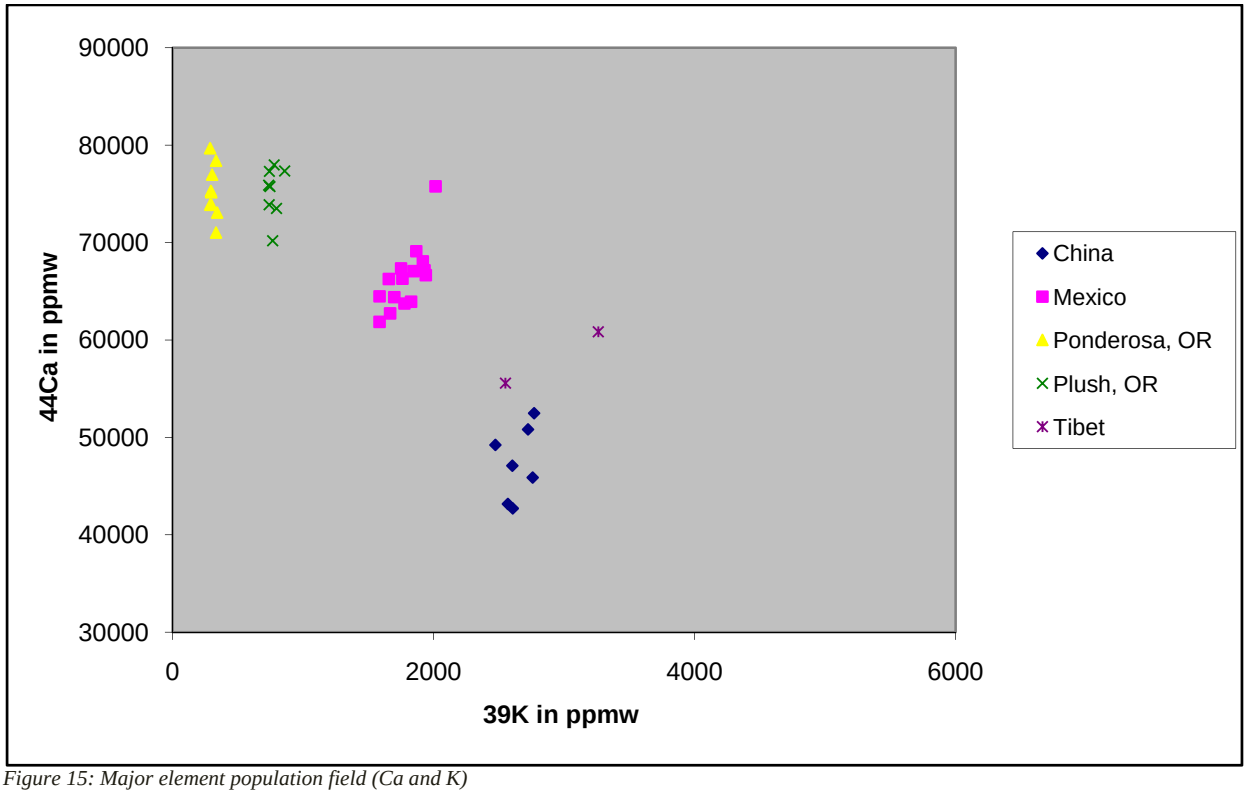

Figure 15: Major element population field (Ca and K)

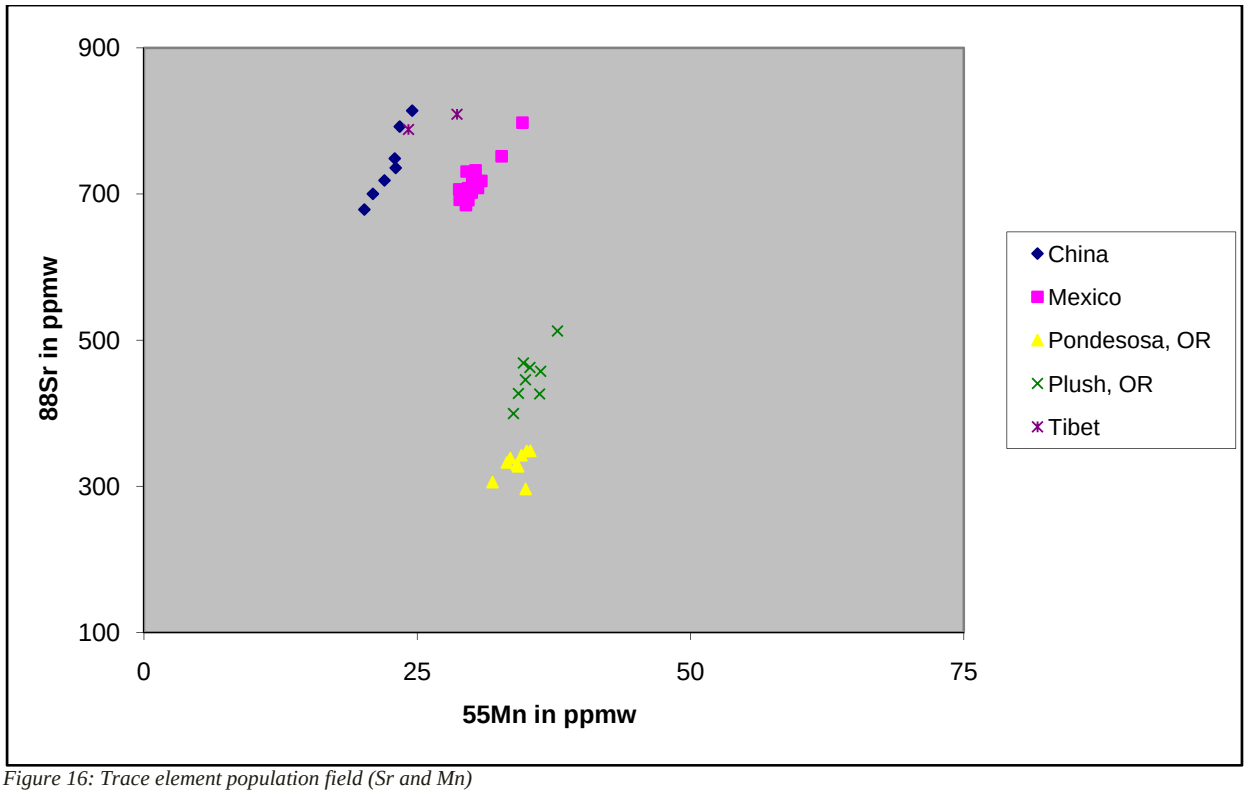

Figure 16: Trace element population field (Sr and Mn)

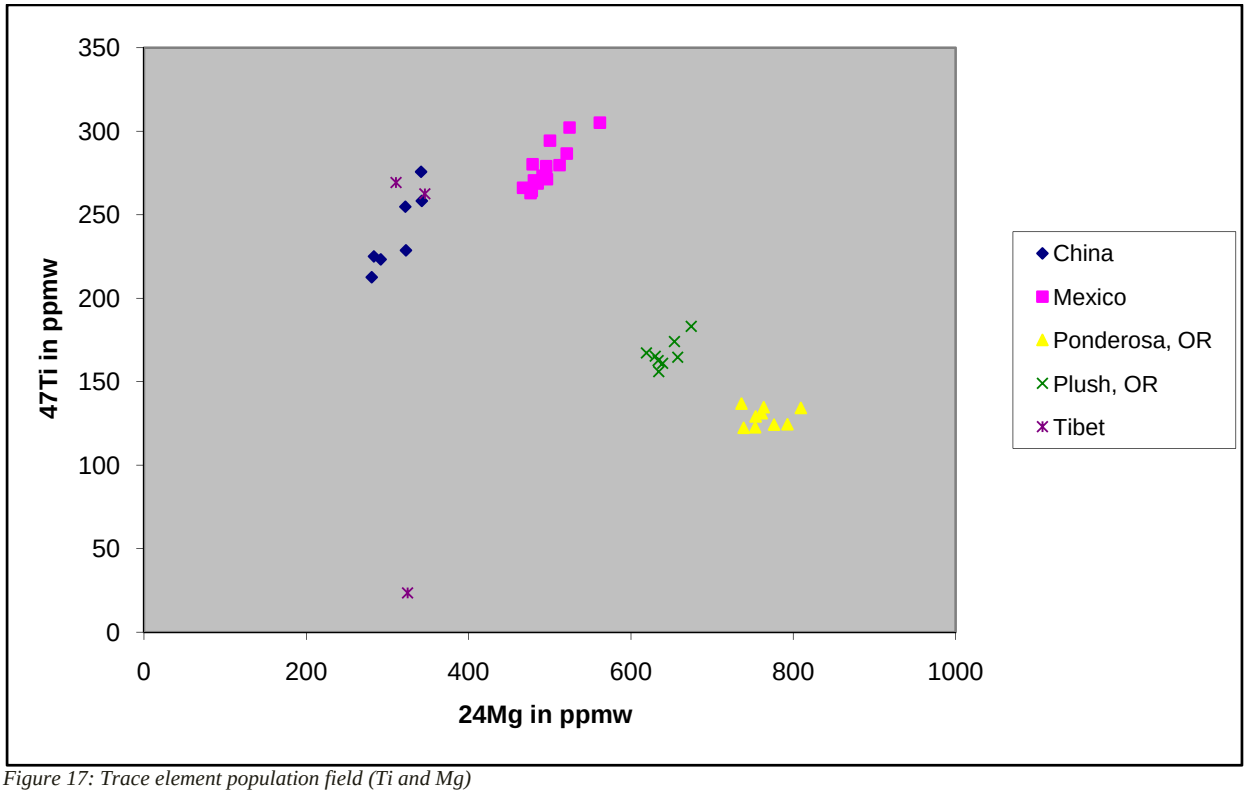

Figure 17: Trace element population field (Ti and Mg)

Most of the elements found can help separating samples from different sources except Mn that did not give a good separation. Some examples of population field plot are

shown in Figure 14 (Fe and Mg), Figure 15 (Ca and K), Figure 16 (Sr and Mn) and Figure 17 (Ti and Mg). All four plots show good separation of samples from Ponderosa, Plush and Mexico. Samples from China and Tibet cluster together but separate from other sources. Plot between Ca and K may be able to help separating the samples from China and Tibet as it shows some separation (Figure 15). However, this aspect will have to be investigated further as the number of samples from Tibet is too small.

Spectroscopy

UV visible NIR spectroscopy

UV/visible/NIR spectra were gained from polished plates for samples from Mexico, Ponderosa, Plush and China. Because of the shape of samples, it was not possible to orientate each of every sample in order to determine alpha, beta and gamma pathlength accurately. Therefore, the plates were orientated with the main polished face perpendicular to the instrument beam and the polarizer was rotated until the maximum difference between spectra was reached. In unheated samples, the spectra show an absorption edge at 300-320 nm, an absorption peak at 381 nm due to Fe^{3+} (Hofmeister and Rossman.1985) and a broad absorption band from 880-1600 nm. In general, the absorption edge increases from 0.5 to 7 nm after heating. The absorption in the 880-1600 nm decreases after heating in samples from Plush and Mexico. But it increases in samples from China except sample 17401892 that showed a decrease. The 381 nm peak does not seem to be effected by heating.

UV/visible/NIR spectra were also gained from the rough Tibet material. The spectra show an absorption edge at 325-340 nm, an absorption peak at 381 nm due to Fe^{3+} and a broad absorption band from 900-1500 nm. There is a 560 nm peak caused by ^{0}Cu particles that are too small too scatter light. The size of the particles are thought to be less than 70 nm (Hofmeister and Rossman. 1985).

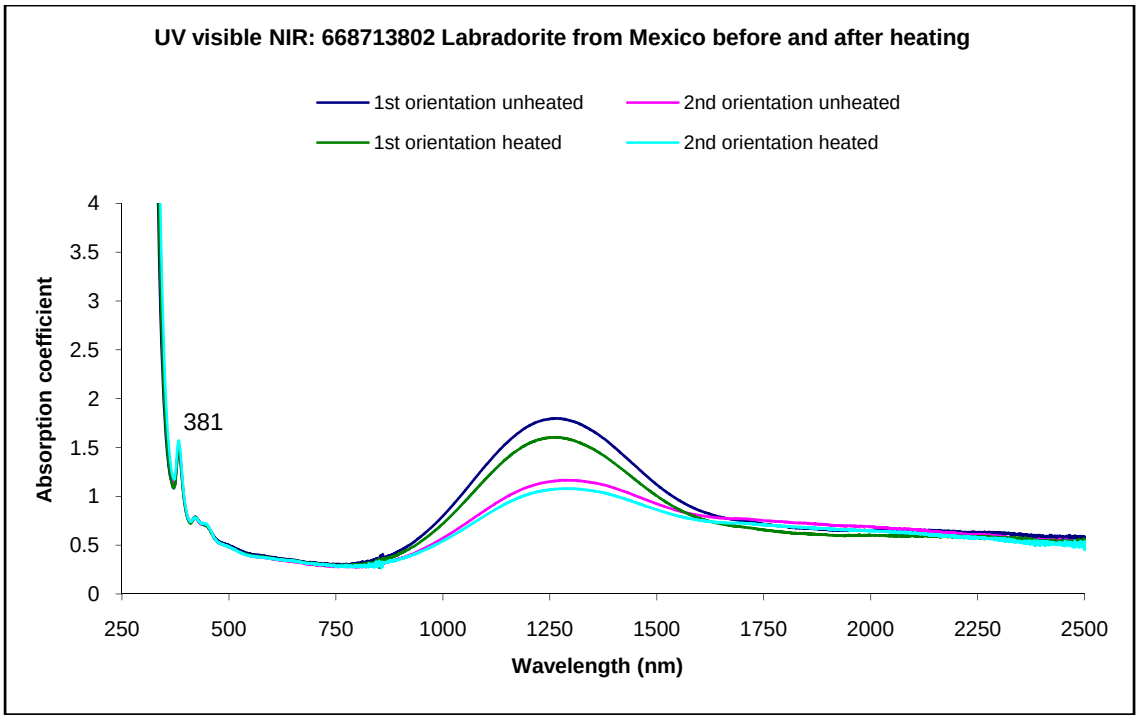

Figure 18: UV visible NIR spectra of labradorite. Absorption edge is around 300-320 nm. Absorption peak at 381 nm is not affected by heat. Absorption in the 880-1600 nm area decreased after heating.

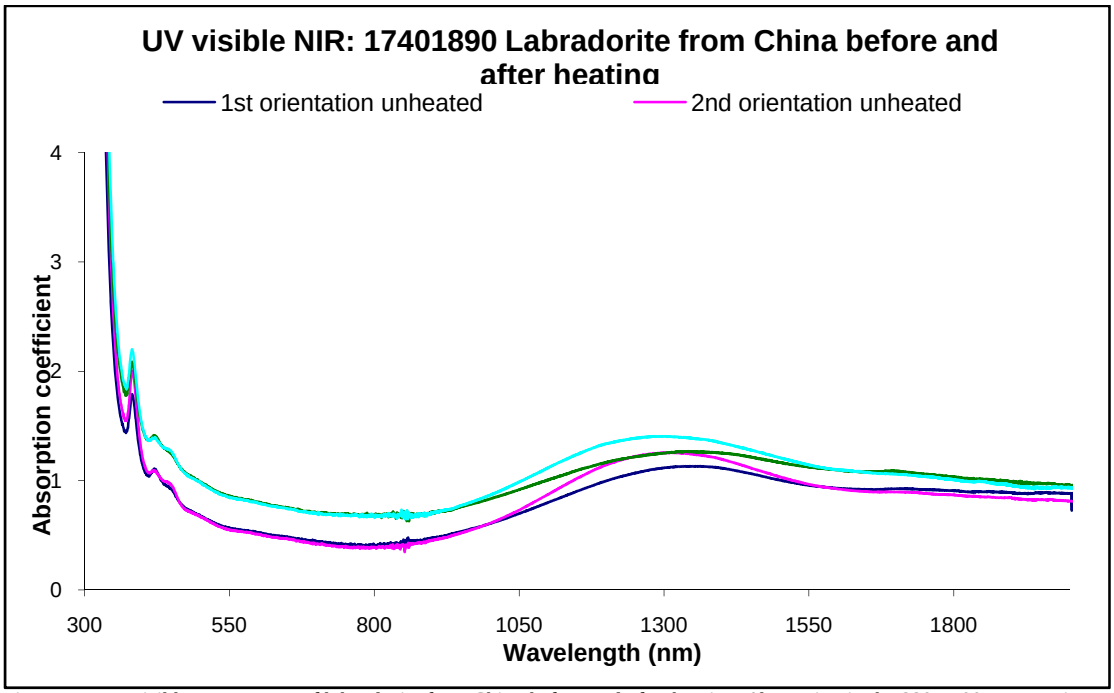

Figure 19: UV visible NIR spectra of labradorite from China before and after heating. Absorption in the 880-1600 nm area increased after heating.

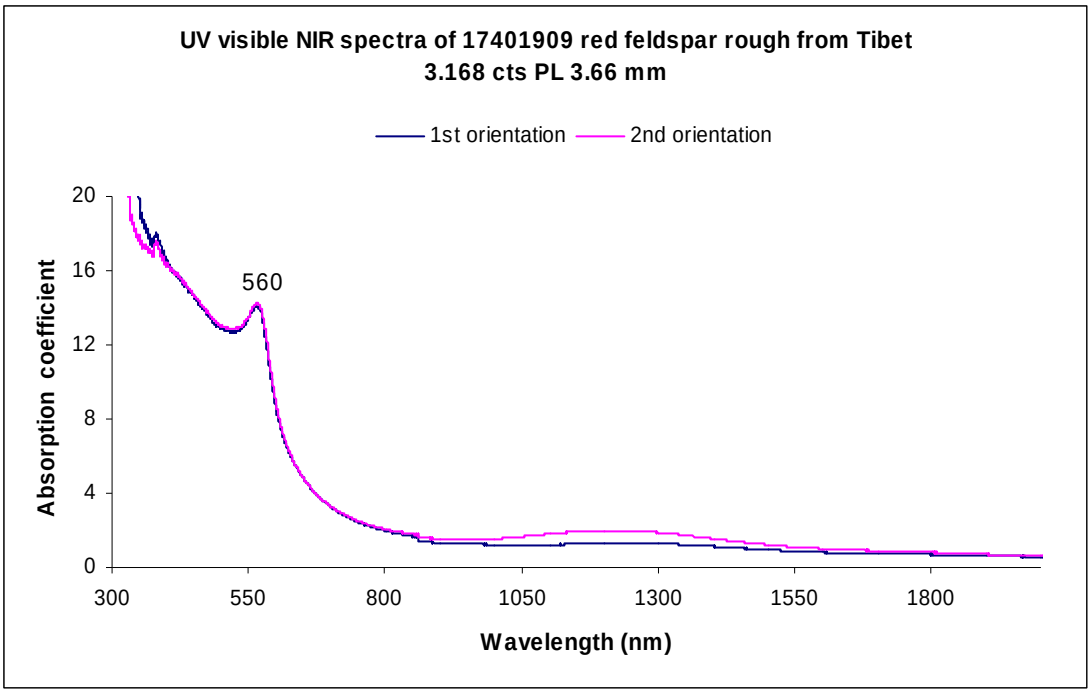

Figure 20: UV visible NIR spectra of red labradorite from Tibet. Absorption peak at 560 nm indicate intrinsic absorption of ^{0}Cu particles. There is an absorption in the 900-1500 nm.

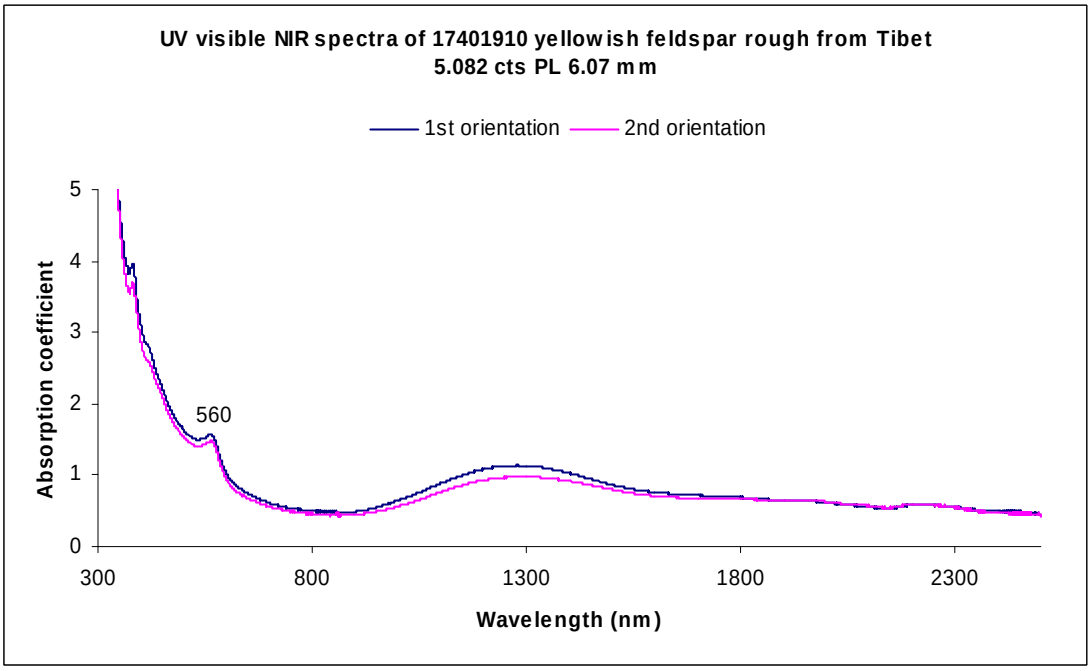

Figure 21: UV visible NIR spectra of yellow labradorite from Tibet. Absorption peak at 560 nm is also present. There is an absorption in the 900-1500 nm.

Infrared spectroscopy

IR spectra showed changes in 3650-2700 cm^{-1} absorption region following heat treatment. Results are shown in Figure 22-28. Many of the samples showed higher absorption while a few samples showed lower absorption. All samples without absorption before heating show an increase in absorption after heating. Unheated samples, 668715902 and 668716002, from Plush, Oregon containing the red schiller cloud showed absorption in this region which decreased after heating (Figure 24 and Figure 25). All three samples from Tibet did not show any absorption in this region. The samples from Ponderosa and Tibet were not subjected to heat treatment at the time, thus, the after heat treatment results are not available for comparison at this point.

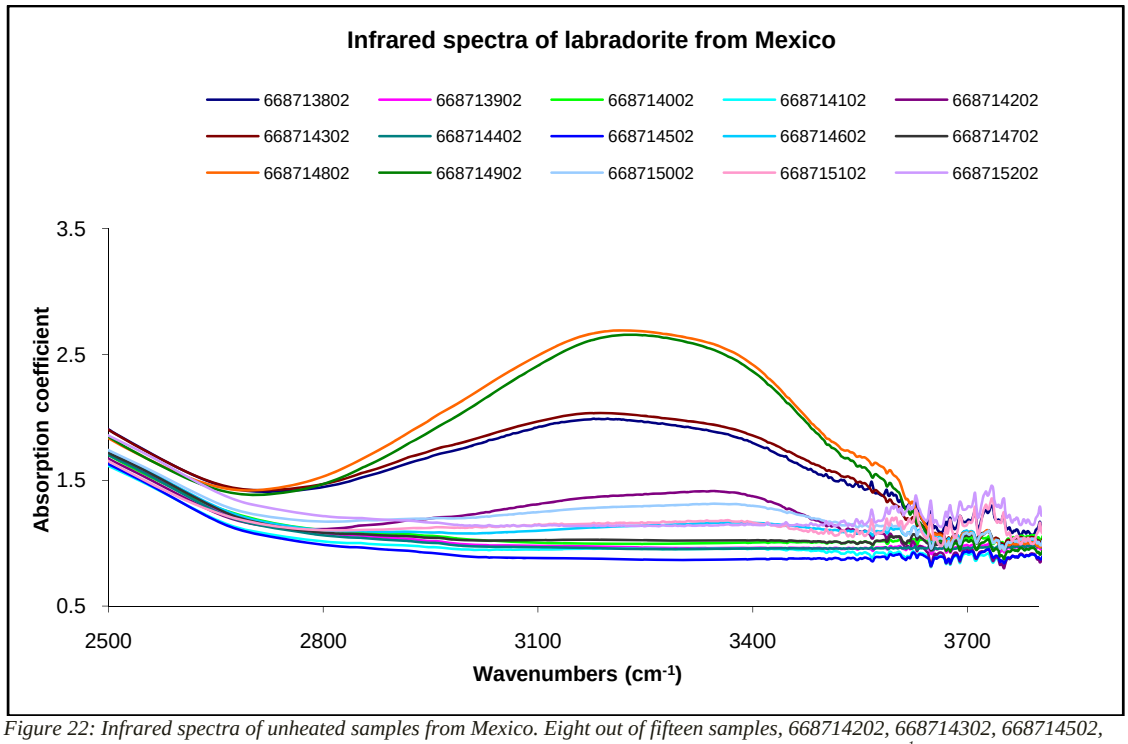

Figure 22: Infrared spectra of unheated samples from Mexico. Eight out of fifteen samples, 668714202, 668714302, 668714502, 668714602, 668714802, 668714902, 668715002 and 668715202 show absorption band at 3650-2700 cm^{-1}.

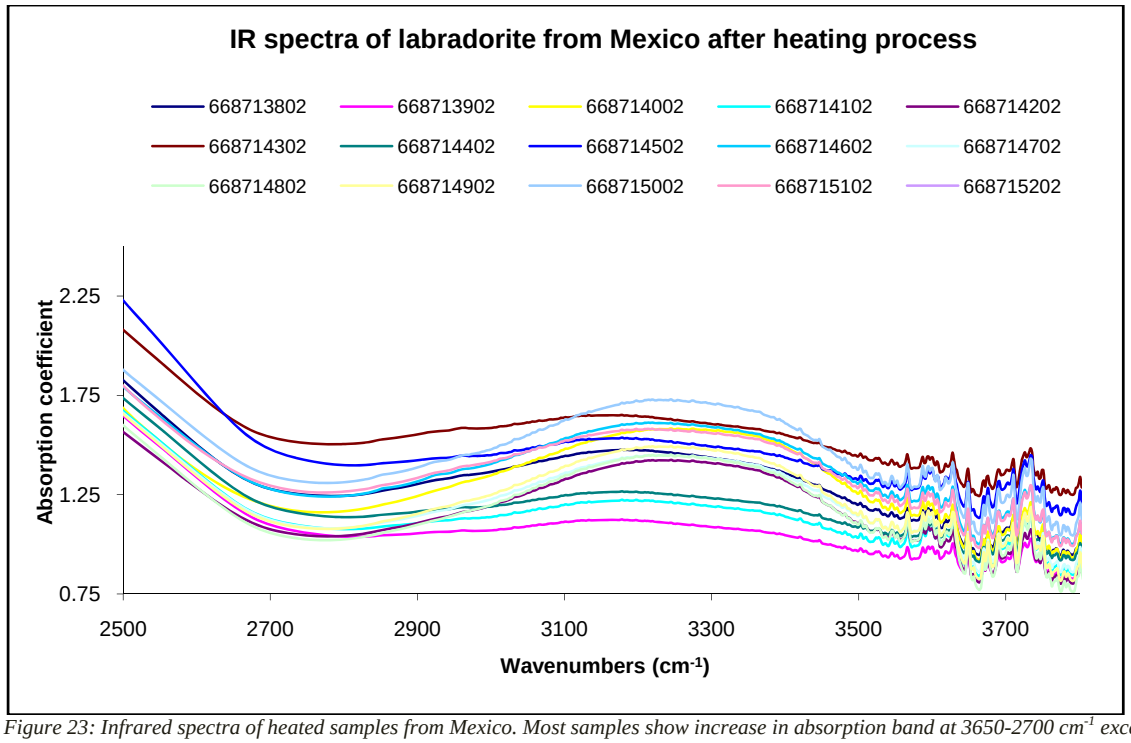

Figure 23: Infrared spectra of heated samples from Mexico. Most samples show increase in absorption band at 3650-2700 cm^{-1} except sample 668713802, 668714302, 668714802 and 668714902. Sample 668714202 shows a shift to the left.

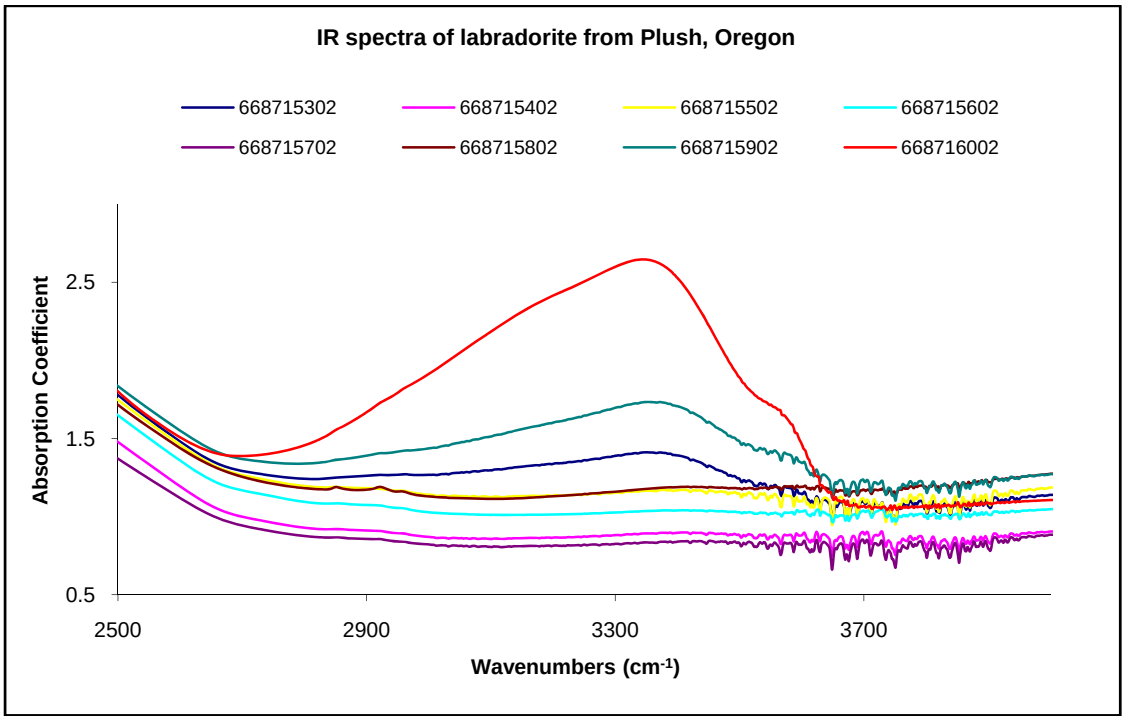

Figure 24: Infrared spectra of unheated samples from Plush, Oregon. Only samples 668715302, 668715902 and 668716002 show absorption band at 3650-2700 cm^{-1}.

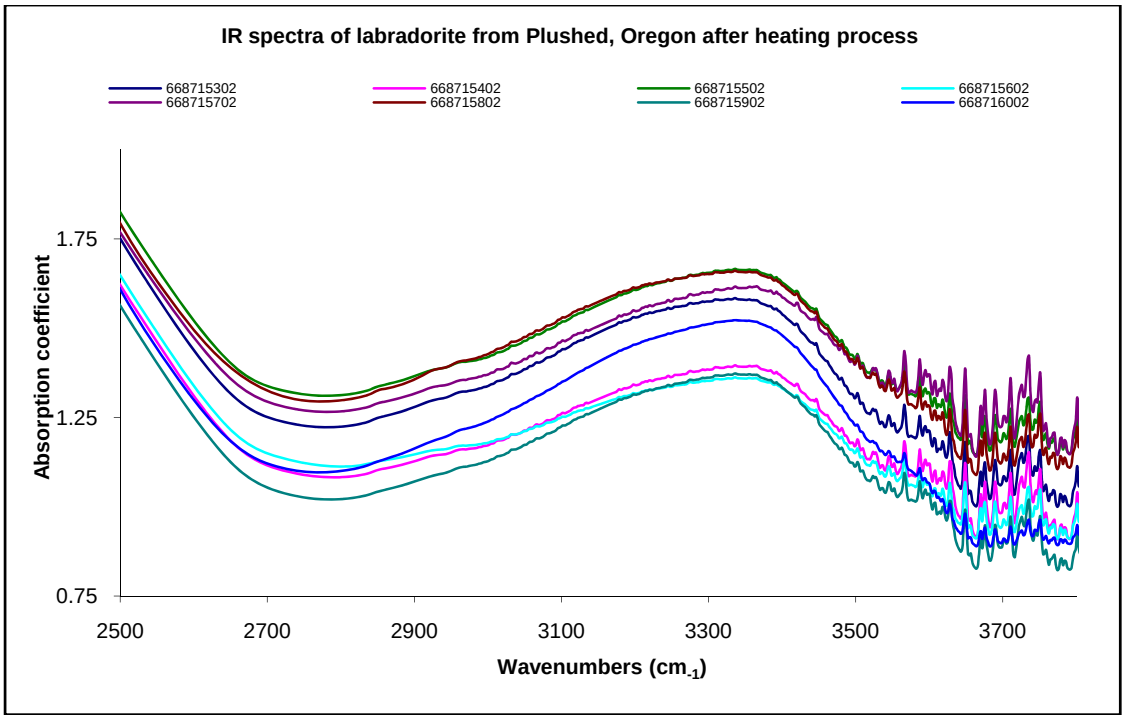

Figure 25: Infrared spectra of heated samples from Plush, Oregon. All samples show an increase in absorption except 668715902 and 668716002 that show a decrease in absorption band at 3650-2700 cm^{-1} after heating.

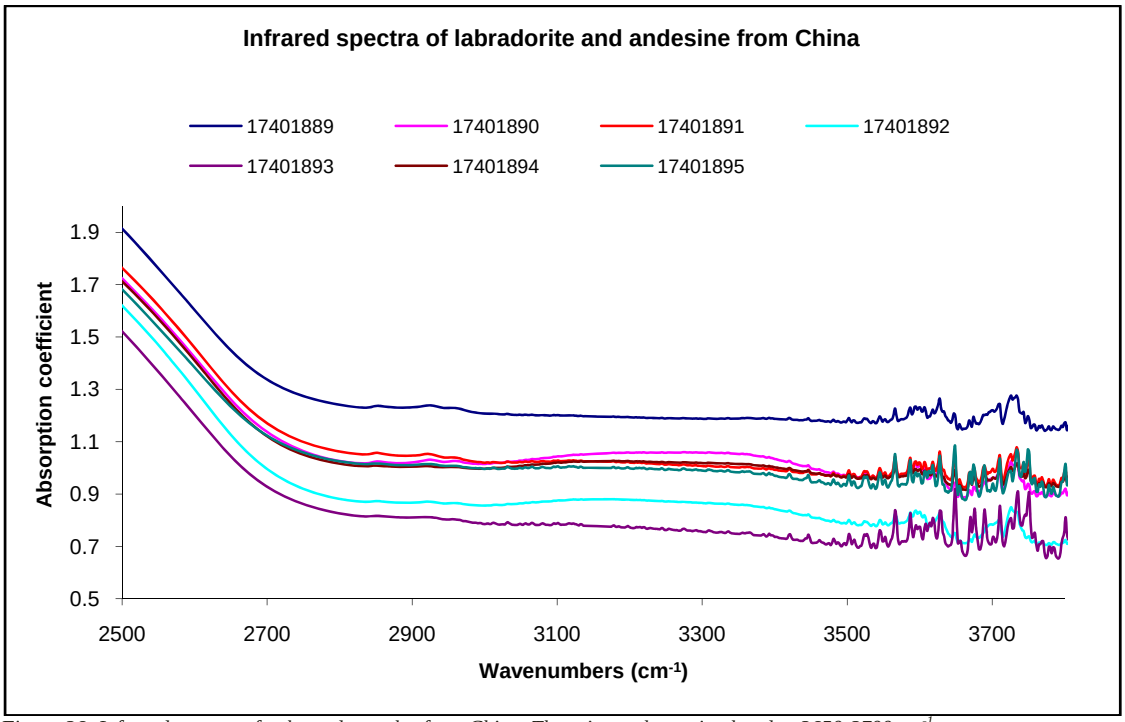

Figure 26: Infrared spectra of unheated samples from China. There is no absorption band at 3650-2700 cm^{-1}.

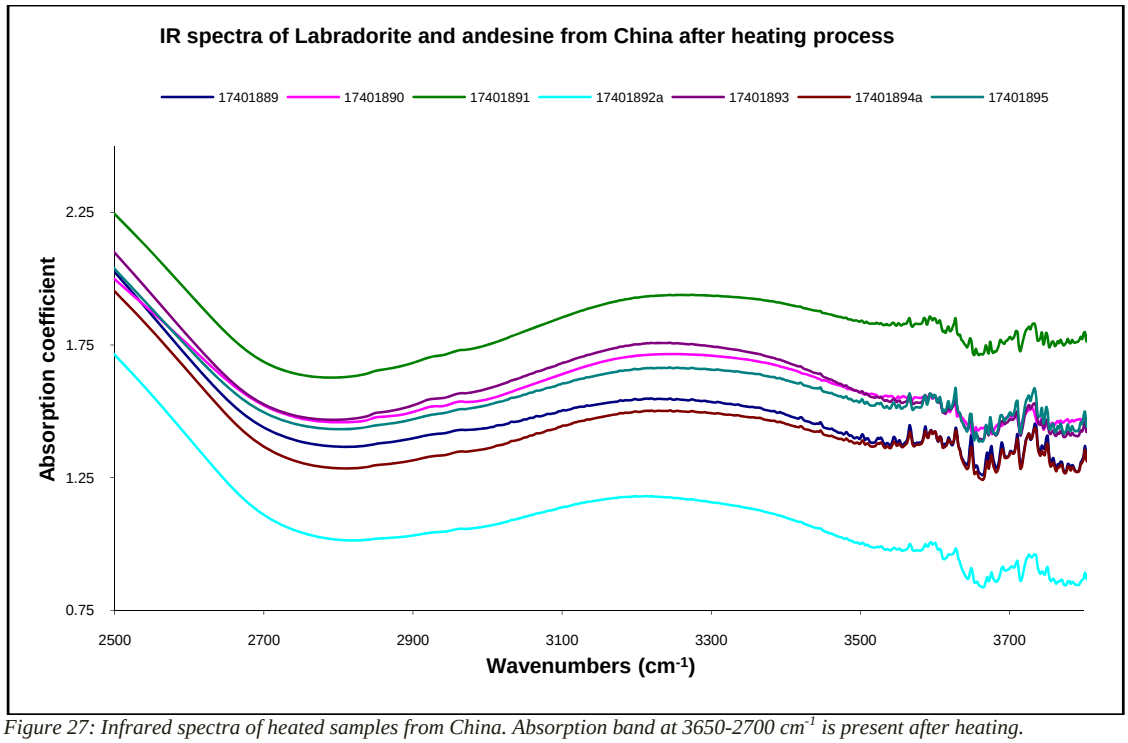

Figure 27: Infrared spectra of heated samples from China. Absorption band at 3650-2700 cm^{-1} is present after heating.

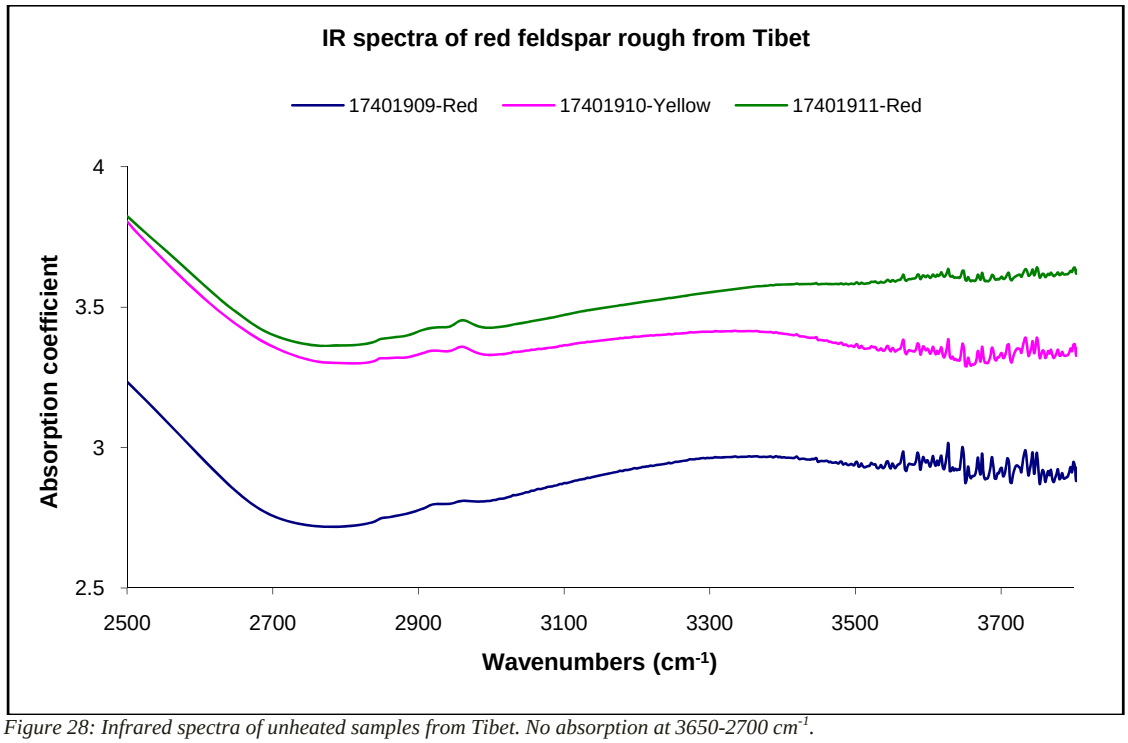

Figure 28: Infrared spectra of unheated samples from Tibet. No absorption at 3650-2700 cm^{-1}.

Inclusion suite

Changes in inclusions were observed under the microscope after heating. For example, deformation of transparent rounded crystals surrounded with healing (Figure 30), discontinuation of tube-like inclusions (Figure 32), reflective discoid fractures that turned milky white (Figure 32), crystals with discoid fractures (Figure 36) and ovoid plates that fused into one large plate after heating (Figure 38), etc.

Photomicrographs of inclusions were taken using Nikon SMZ 1500 system attached to a modified base of GIA Gem microscope and NIS-Elements D 2.30 application. The photomicrographs were taken under dark-field, bright-field and oblique illumination.

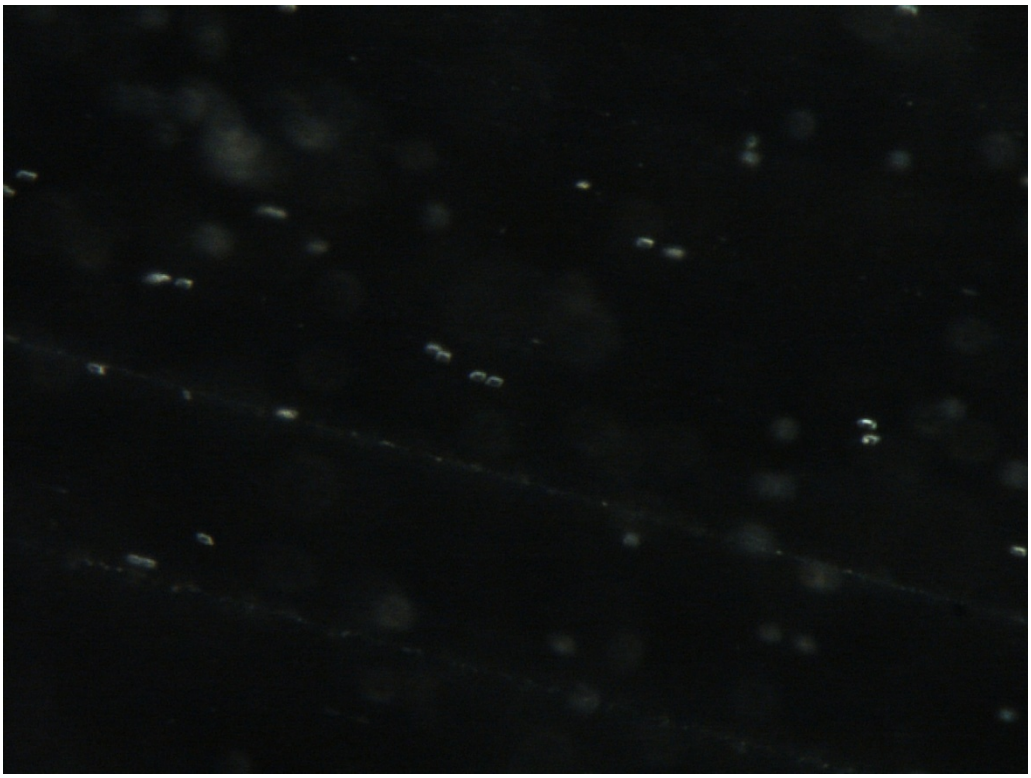

Figure 29: Transparent rounded uniform crystals occur in pairs before heating (17401892). See Figure 30, note the differences after heating.

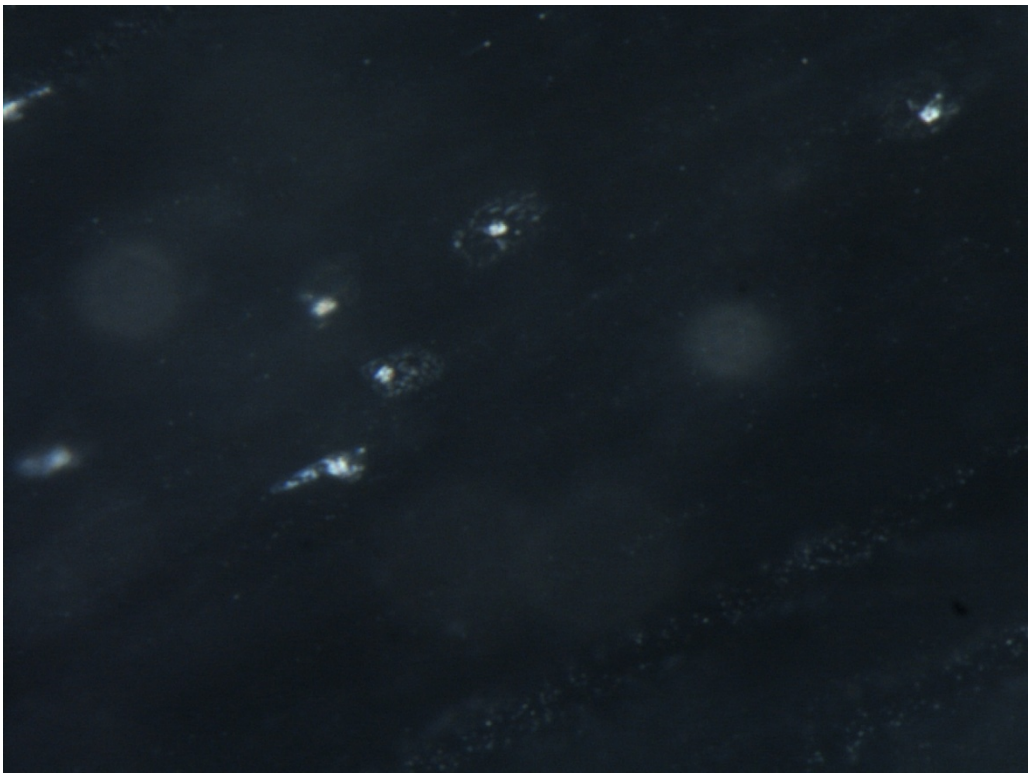

Figure 30: Deformation of the transparent rounded crystals surrounded with healing after heating (17401892). See Figure 29, note the differences before heating.

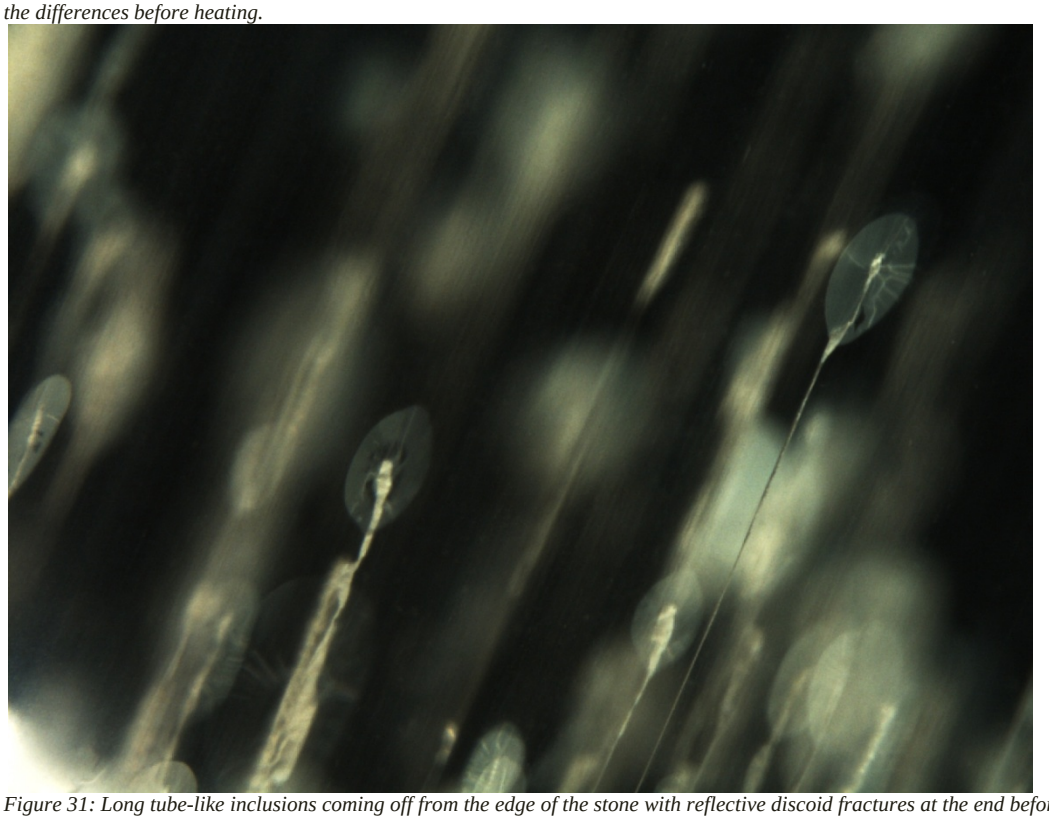

Figure 31: Long tube-like inclusions coming off from the edge of the stone with reflective discoid fractures at the end before heating (17401895). See Figure 32, note the differences after heating.

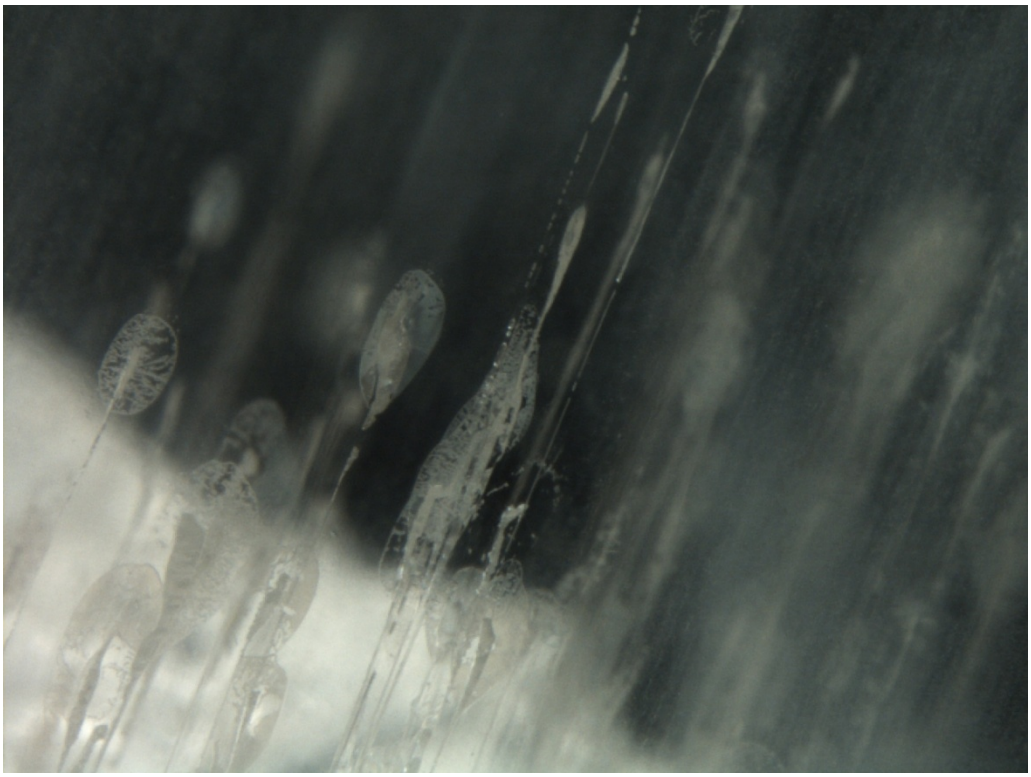

Figure 32: Discontinuation of the tube-like inclusion possibly recrystalization of feldspar filling the hollow structure. The reflective discoid fracture turned milky white after heating (17401895). See Figure 31, note the differences before heating.

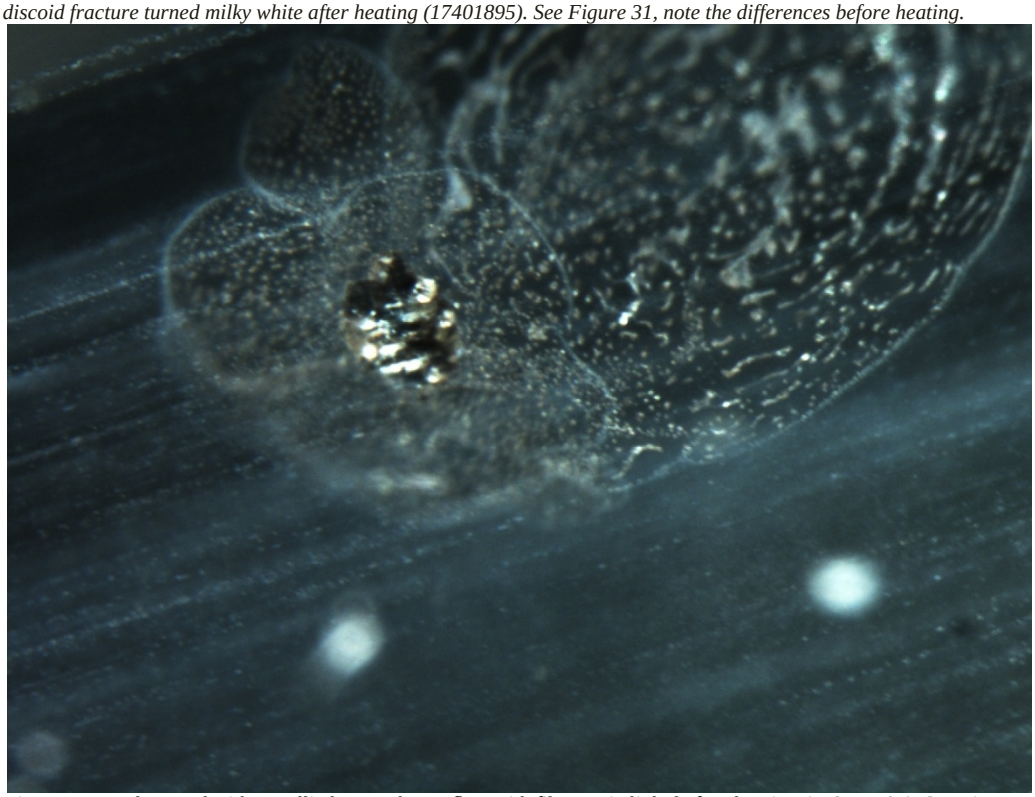

Figure 33: Dark crystal with metallic luster when reflect with fiber optic light before heating (668714202). See Figure 34, note the differences after heating.

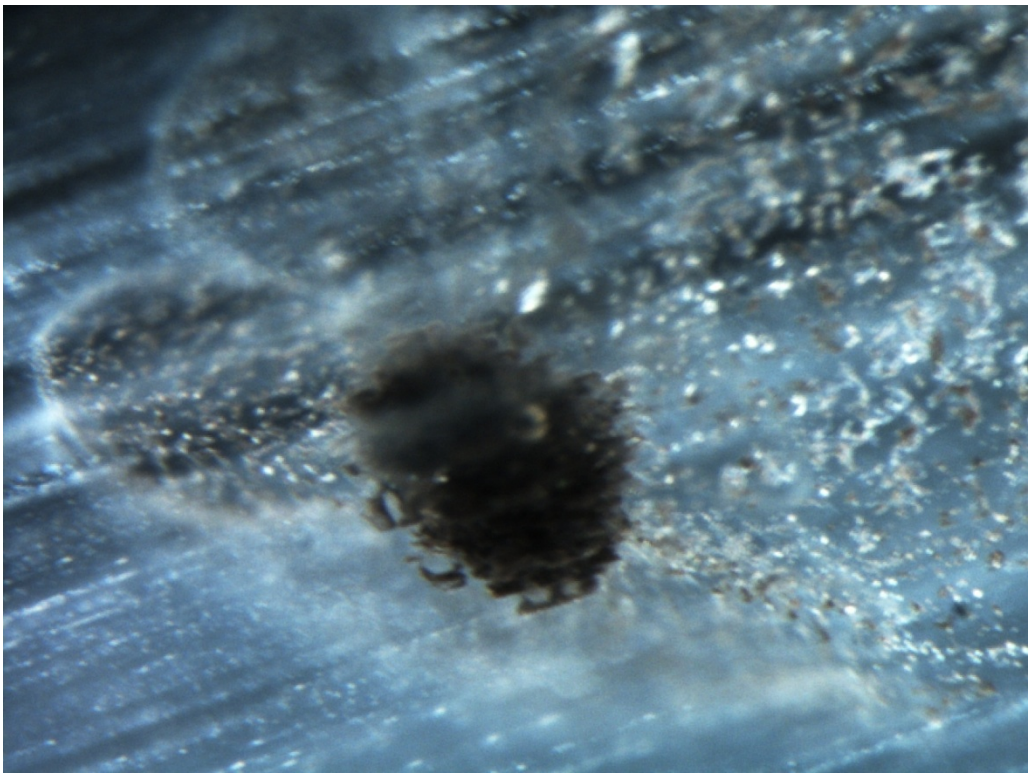

Figure 34: The dark crystal lost its luster and disintegration on the surface occurred after heating (668714202). See Figure 33, note the differences before heating.

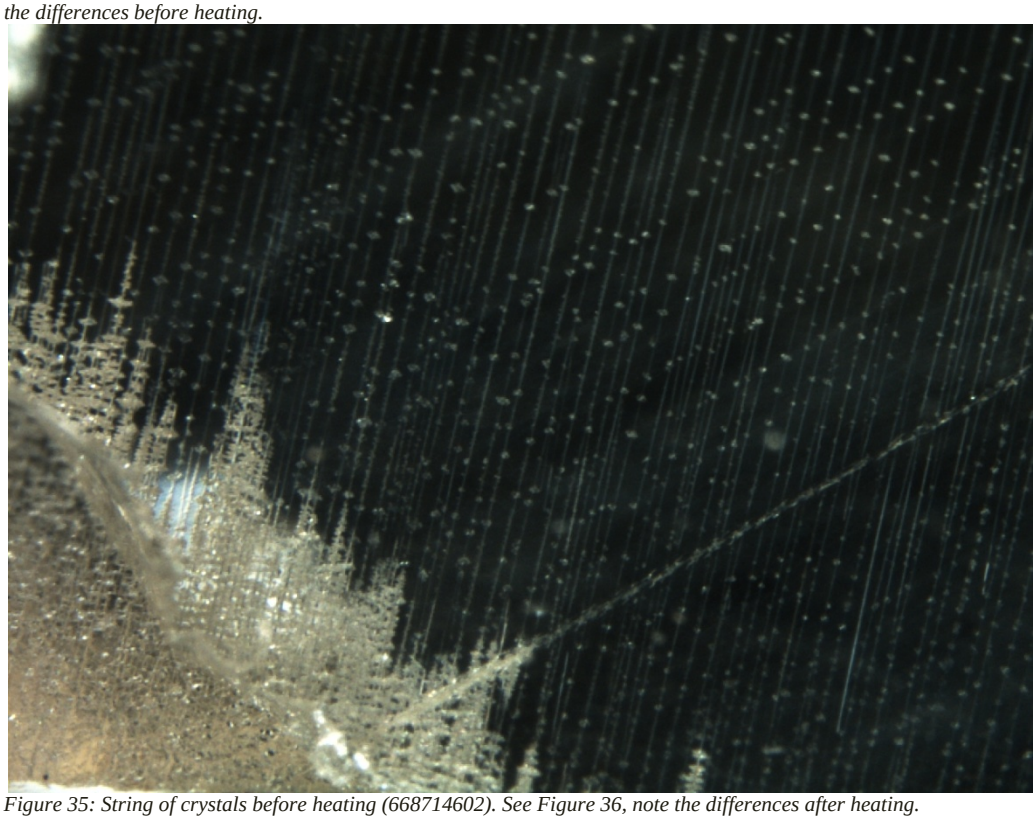

Figure 35: String of crystals before heating (668714602). See Figure 36, note the differences after heating.

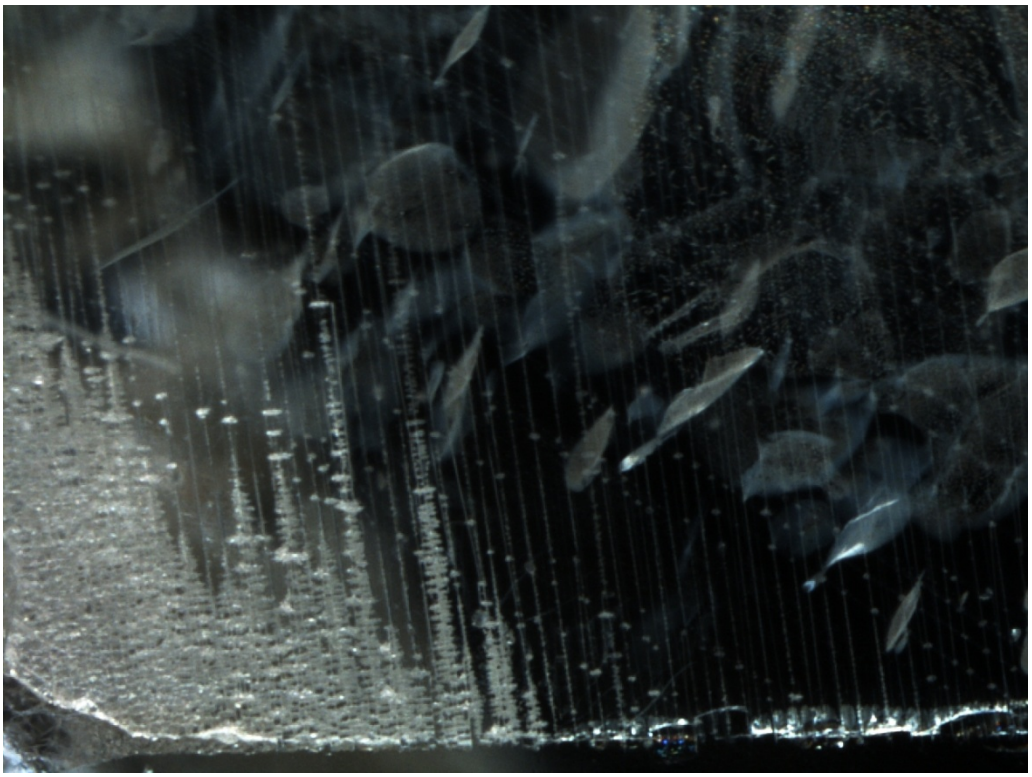

Figure 36: String of crystals with large discoid fractures which occurred after heating (668714602). See Figure 35, note the differences before heating.

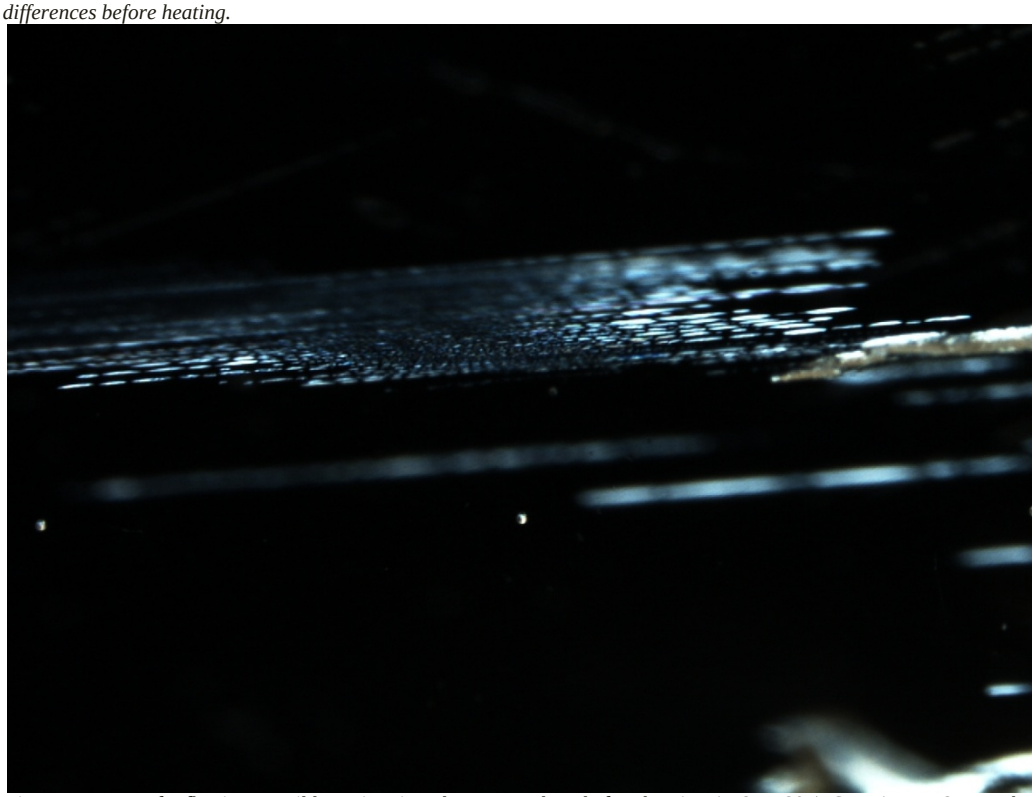

Figure 37 Rows of reflective, possible peristerite, plates on a plane before heating (668714802). See Figure 38, note the differences after heating.

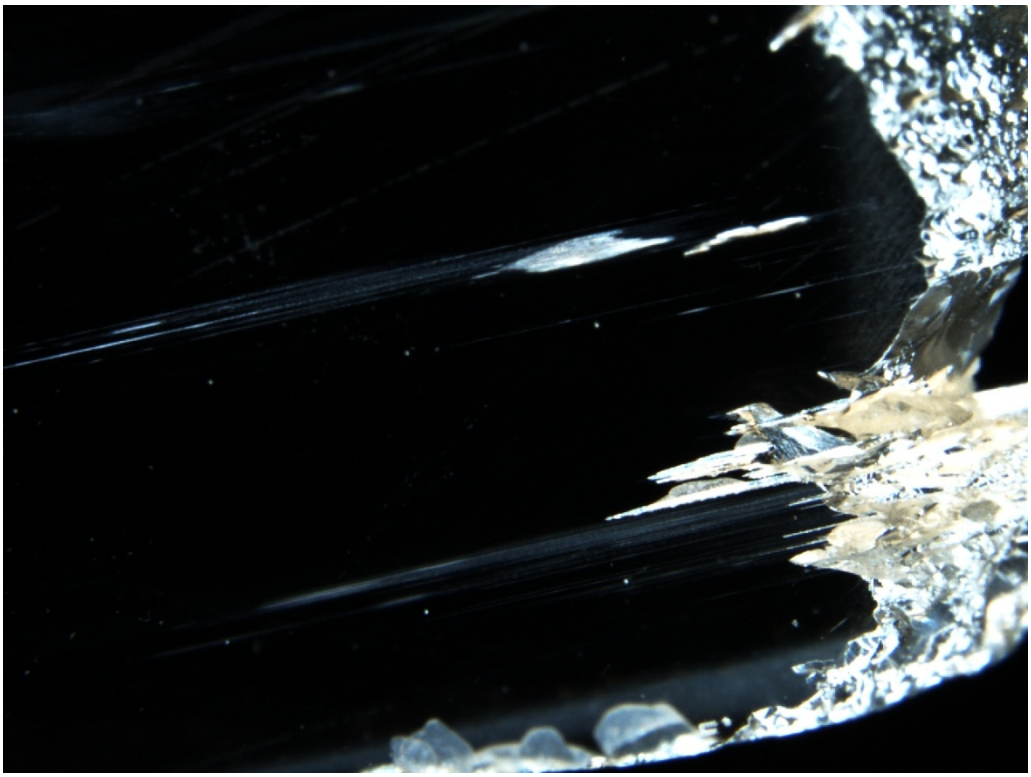

Figure 38: The reflective plates fused into one large rounded plate after heating (668714802). See Figure 37, note the differences before heating.

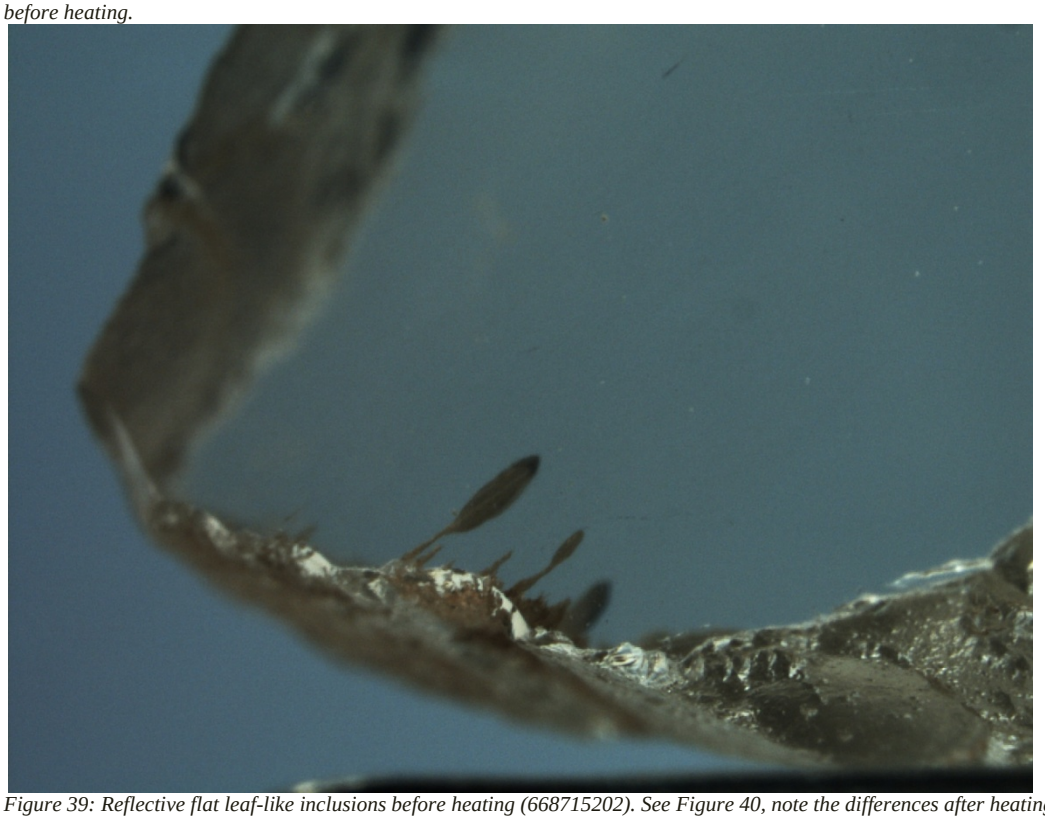

Figure 39: Reflective flat leaf-like inclusions before heating (668715202). See Figure 40, note the differences after heating.

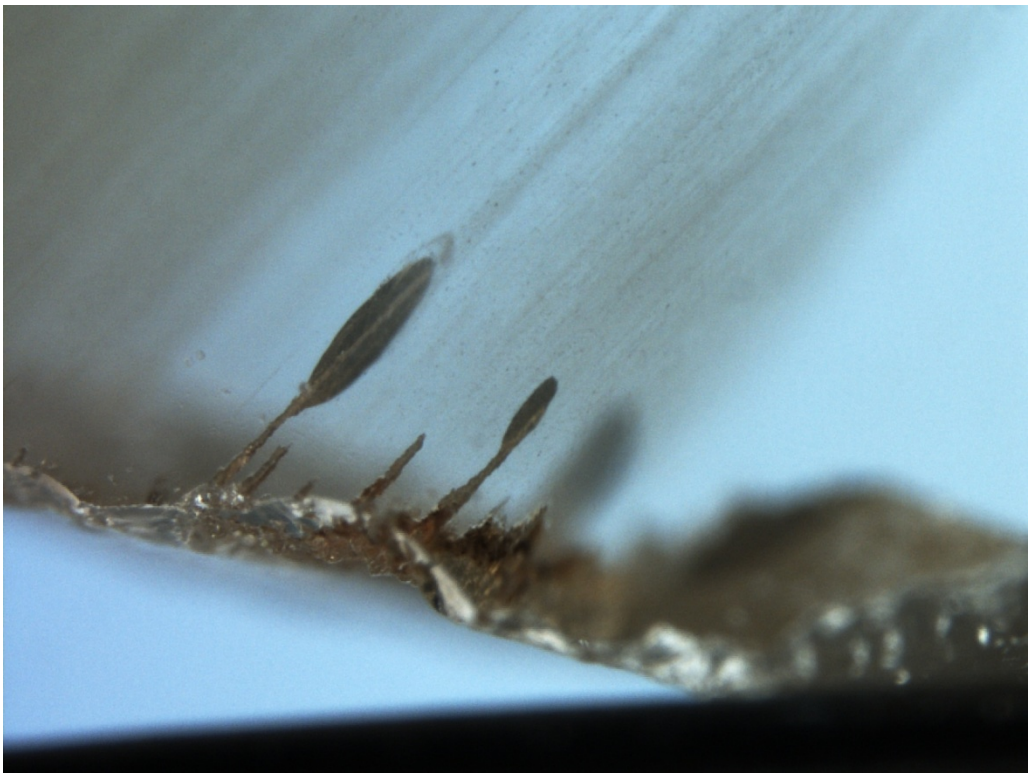

Figure 40:: A fracture appeared at the top after heating (668715202). See Figure 39, note the differences before heating.

Surface examination of the red feldspar rough from Tibet

The surface of the red feldspar rough is pitted with some areas that appear melted. Upon close examination, glassy surface and clusters of transparent crystals (Figure 42) were observed. Identification of these is presently being worked on.

Figure 41 Surface of sample 17401909 from Tibet. The area appears melted with smooth glassy surface and clusters of transparent crystals. Photo by Garry Du Toit.

Discussion

At this point of the investigation, it seems that changes caused by heat treatment may be identified using a gemological microscope. The changes in inclusions seem to be the best means of determining heat treatment. Chemical analysis using LA-ICP-MS proves to be a very useful method in identifying sources of material as they have distinct differences in their chemical composition. It was interesting that the red schiller cloud lost its red coloration due to heating at 1200 °C for 50 hours along with internal diffusion of Cu. Optical data did not prove to be useful in this examination as the changes detected are not consistent. The samples are now in the process of Cu diffusion and will be reexamined.

Acknowledgements

The author thanks John L. Emmett and Ahmadjan Abduriyim for the samples, Sudarat Saeseaw for LA-ICP-MS analysis. Additionally thanks are due to Kenneth Scarratt, Garry Du Toit, Nicholas Sturman and Vincent Pardieu for their suggestions in this study.

With the collaboration of John L. Emmett, this study continues and once sufficient data has been collected and studied a joint paper will be published.

References

Mernagh, T. T. (1991) Use of the Laser Raman Microprobe for Discrimination Amongst Feldspar Minerals. *Journal of Raman Spectroscopy*. 22. 453-457

Freeman, J. J., et al. (2008) Characterization of Natural Feldspars by Raman Spectroscopy for Future Planetary Exploration. *The Canadian Mineralogist*. 46. 1477-1500

Hofmeister, A. M., et al. (1985) Exsolution of metallic copper from Lake County labradorite. *Geology*. 13. 9. 644-647

Pearce, N. J. G., Perkins, W.T., Westgate, J.A., Gorton, M.P., Jackson, S.E., Neal, C.R., Chenery, S.P. (1996) Application of new and published major and trace elements data for NIST SRM 610 and NIST SRM 612 glass reference materials. *Geostandards Newsletter*. 20 2. 115-144